An Adaptive Control Technology for Flight Safety in the Presence of Actuator Anomalies and Damage

by

Megumi Matsutani

Submitted to the Department of Aeronautics and Astronautics
in partial fulfillment of the requirements for the degree of

Master of Science in Aeronautics and Astronautics Engineering

at the

MASSACHUSETTS INSTITUTE OF TECHNOLOGY

[February 2010]
Jan 2010

Author .....
Department of Aeronautics and Astronautics
Jan 15, 2010

Certified by .....
Dr. Anuradha Annaswamy
Senior Research Scientist
Thesis Supervisor

Accepted by .....
Prof. Eytan H. Modiano
Associate Professor of Aeronautics and Astronautics
Chair, Committee on Graduate Students

An Adaptive Control Technology for Flight Safety in the Presence of Actuator Anomalies and Damage

by

Megumi Matsutani

Submitted to the Department of Aeronautics and Astronautics
on Jan 15, 2010, in partial fulfillment of the
requirements for the degree of
Master of Science in Aeronautics and Astronautics Engineering

Abstract

The challenge of achieving safe flight comes into sharp focus in the face of adverse conditions caused by faults, damage, or upsets. When these situations occur, the corresponding uncertainties directly affect the safe operation of the aircraft. A technology that has the potential for enabling a safe flight under these adverse conditions is adaptive control. One of the main features of an adaptive control architecture is its ability to react to changing characteristics of the underlying aircraft dynamics. This thesis proposes the building blocks of an adaptable and reconfigurable control technology that ensures safe flight under adverse flight conditions. This technology enables the synthesis of such controllers as well as the systematic evaluation of their robustness characteristics.

The field of adaptive control is a mature theoretical discipline that has evolved over the past thirty years, embodying methodologies for controlling uncertain dynamic systems with parametric uncertainties [1, 2, 3, 4, 5, 6]. Through the efforts of various researchers over this period, systematic methods for the control of linear and nonlinear dynamic systems with parametric and dynamic uncertainties have been developed [7, 8, 9, 10, 11, 12]. Stability and robustness properties of these systems in the presence of disturbances, time-varying parameters, unmodeled dynamics, time-delays, and various nonlinearities, have been outlined in the references [4]-[13] as well as in several journal and conference papers over the same period.

In this thesis, we consider the control of a transport aircraft model that resembles the Generic Transport Model [14]. While the vehicles' geometry and aerodynamic model are those of a C5 aircraft, every other aspect has been made to coincide with the GTM, e.g. anti wind-up logic, time-delay due to telemetry, baseline control structure, low-pass and wash-out filters. We delineate the underlying nonlinear model of this aircraft, and introduce various damages, and failures into this model. An adaptive control architecture is proposed which combines a nominal controller that provides a satisfactory performance in the absence of adverse conditions, and an adaptive controller that is capable of accommodating various adverse conditions including actuator saturation. The specific adverse conditions considered can be grouped into the

following three categories, (a) upsets, (b) damages, and (c) actuator failures. Specific cases in (a) include flight upsets in initial conditions of various states including angle of attack, cases in (b) include situations where structural failures cause changes in the location of the Center-of-Gravity (CG)[15], while cases in (c) include situations where symmetric and asymmetric failures in control surfaces and engines occur. These failures include losses in control effectiveness, and locked-in-place control surface deflections.

The resilience of the adaptive controller to uncertainty is evaluated for safety using the control verification methodology proposed in [16]. This methodology enables the determination of ranges of uncertainty for which a prescribed set of closed-loop requirements are satisfied. This thesis studies several one-dimensional uncertainty analyzes for two flight maneuvers that focus on the longitudinal and lateral dynamics. As compared to the baseline controller, the adaptive controller enlarges the region of safe operation by a sizable margin in all but one of the cases considered.

Thesis Supervisor: Dr. Anuradha Annaswamy
Title: Senior Research Scientist

Acknowledgments

Firstly, I would like to acknowledge my advisor Anuradha Annaswamy for educating and guiding me to conduct great research, giving me an opportunities to visit Technische Universitat Munchen in the spring of 2009 and NASA Langley Research Center in the summer of 2008 and 2009, and to have fruitful research interactions there. I would like to thank Luis G. Crespo at National Institute of Aerospace for many insightful discussions and for the support in conducting simulation studies. I would also like to thank to NASA IRAC project for supporting this work. Lastly, I want to thank my best friend Beni Yoshida for his support.

Contents

List of Figures

List of Tables

Chapter 1

Introduction

1.1 Adaptive Flight Control

1.1.1 Adaptive Control

The field of adaptive control has addressed the problem of control of dynamic systems with parametric uncertainty [1]-[5],[17]. The simplest example is the control of a plant having the form

$$y = (W_p(s, \theta_0))u \tag{1.1}$$

where $W_p(s)$ represents the aircraft dynamics linearized about a trim condition, θ_0 is the nominal value of the uncertain parameter θ, and u and y represent a vector of control inputs and measurable outputs. We will assume that θ belongs to the set, $H(\theta_0, \lambda)$ where λ, the uncertainty radius, is proportional to the uncertainty we have in the actual value of θ. $H(\theta_0, \lambda)$ may be due to uncertain aerodynamic coefficients, inaccurate atmospheric models, or actuator failures. The adaptive controller is given by

$$u = C(k(t), y, \delta, \Gamma) \tag{1.2}$$

where $k(.)$ is a control parameter that is varied nonlinearly as a function of on-line measurements of the vehicle, δ is a vector of command signals, and Γ is an adaptation gain. It is well known that the closed-loop system is guaranteed to be stable, and that the output tracks specified command signals arbitrarily closely under certain matching conditions. Yet another uncertainty that can be addressed is due to unmodeled dynamics whose effects may be due to atmospheric excitation, or flutter modes. If these effects are represented through the operator $\mu\Delta(s)$, where $\Delta(s)$ has a bounded norm and μ is a finite gain, the vehicle dynamics is now given by

$$y = (W_p(s,\theta) + \mu\Lambda(s))u. \tag{1.3}$$

For every uncertainty model H, choice of an adaptation gain Γ, command signal δ and performance metric, there exists a critical gain $\mu^\star$, that can be tolerated [4]. Bounds of $\mu^\star$ have been derived for general uncertainties $\Delta(s)$.

1.1.2 On-line Reallocation in the Presence of Actuator Failures

The advantage of any adaptive control system is its ability to cope with unforeseen changes in the flight and environmental dynamics. Possible causes of such changes are actuator failure, vehicle geometry changes, and other disturbances. In [10], a direct-adaptive flight controller is proposed to enable reconfiguration in the presence of actuator failures, environmental disturbances, and modeling errors. The controller, developed using the K&A algorithm in [7] enables stable compensation in the presence of actuator failures via on-line reconfiguration and control allocation, while accommodating for magnitude constraints on the control input. For the system in (1.3), an adaptive controller which incorporates reallocation over control surfaces is designed as

$$u = G(G_0, x, t, x_{\text{cmd}}) \tag{1.4}$$

where G is a nonlinear reallocation algorithm which depends on G_0, a constant reallocation matrix, x is the state, and x_{cmd} is a command signal. Benefits of the proposed adaptive controller were demonstrated using a linearized six-degree of freedom simulation model of a large, four engine transport aircraft. It was observed that this algorithm provides improved performance compared to a standard adaptive algorithm.

1.2 Control Verification & Validation

1.2.1 Control Verification Methodology

The set of design requirements to be satisfied by the closed-loop system can be described by a collection of inequality constraints that depend on the uncertain parameters and the design variables. In general, these requirements can be prescribed as

$$g(\theta, t, d, \mu, \Delta) < 0 \tag{1.5}$$

where d is the design variable. The projection of the constraint in (1.5) onto the θ-space partitions the uncertain space into two regions, a region where the constraint is violated, called the Failure Domain F, and a region where the constraint is satisfied, called the Safe Domain. Depending on the requirement being cast by Equation (1.5), excursions into the Failure Domain could represent instability, poor handling qualities, or excessive control actuation.

The Parametric Safety Margin, whose evaluation requires the homothetic deformation of the set $H(\theta_0, \lambda)$, is the "distance between $H(\theta_0, \lambda)$ and the Failure Domain. This deformation, which uses θ_0 as an anchor point while preserving the orientation and proportionality of H, is performed until the deformed set touches the boundary of the Failure Domain. The resulting deformed set is called the Maximal Set. The Parametric Safety Margin is a measure of the size of the Maximal Set. The larger the Parametric Safety Margin, the larger the smallest excursion from θ_0 required for

violating Equation (1.5), thus, the better the robustness.

When Equation (1.5) casts the stability and performance requirements on the closed-loop system, the Parametric Safety Margins unambiguously characterizes the resilience of the adaptive controller to uncertainty in θ. A methodology for robustness analysis and robust design, based on Parametric Safety Margins, has been proposed in [18]. These robustness metrics can be used to evaluate the ability of control systems to satisfy the closed-loop stability and performance requirements in the presence of uncertain physical parameters, control failures, and damage. Because this framework is applicable to nonlinear, possibly time-varying systems, where requirements that explicitly depend on time are present, these metrics are well suited for adaptive control.

The Parametric Safety Margins can also be used to systematically "robustify adaptive controllers. By this we mean that we can search for a control architecture so that the set of free parameters maximize the robustness margins. This thesis does not tackle such a optimization problem though and applies the metrics only to the robustness study of the adaptive control architecture to be designed in this thesis and to the evaluation of the improvement in flight safety attained by adaptation.

1.2.2 Generic Transport Model

The Generic Transport Model (GTM) is a dynamically scaled model of a transport aircraft for which NASA Langley has developed a high-fidelity simulink model. This simulation uses non-linear aerodynamic models extracted from wind tunnel data, and considers avionics, sensor dynamics, engine dynamics, atmospheric models, sensor noise and bias, telemetry effects, etc. This aircraft has ten controllable inputs and overall the open-loop plant has 278 states. As the actual vehicle itself, this model departs considerably from the Linear Time Invariant (LTI) system usually assumed for control design and therefore enables us to determine whether the improvements in stability, safety, and performance expected can be realized in practice. Using this vehicle, conducting a flight test is one of our plans to validate an adaptive control technology for flight safety. As well as the studies to be conducted in this thesis, this

strongly connects this mature theoretical discipline of adaptive control to the actual world, and leads to realization of actual applications of adaptive control on aerospace applications to achieve a safety flight.

1.3 Organization of this Thesis

In this thesis, we start with building the nonlinear dynamic model of C5, a large transport aircraft in Chapter 2. For this GTM-like model, we design an adaptive control architecture in Chapter 3. With the control verification metrics which is to be introduced in Chapter 4, we then evaluate the robustness of the adaptive system to uncertainties in Chapter 5. Based on the studies from the previous chapters, Chapter 6 presents developments of an adaptive controller for the GTM. Finally Section 7 summarizes the thesis.

Chapter 2

The Model of a Large Transport Aircraft

In this chapter, we begin with a description of the nonlinear dynamic model of C5, a large transport aircraft whose aerodynamics data is available in [19]. We consider rigid body dynamics, aerodynamics, the effect of the control inputs and derive the overall nonlinear flight model. We then discuss adverse conditions such as flight upsets, damages, and failures, and how to model them.

2.1 Nonlinear Dynamic Model

A typical dynamic model of an aircraft consists of the equations of motion, aerodynamics, actuator dynamics, actuator saturation, and sensor dynamics. The standard conservation equations [20] describe the dynamics of u, v, and w, the body-fixed aircraft velocities; p, q, and r, the roll, pitch, and yaw rates; and the Euler angles ϕ, θ, and ψ. The aircraft's equations of motion are given by

$$\dot{u} = g\frac{X}{W} - g\sin\theta - qw + rv, \tag{2.1}$$

$$\dot{v} = g\frac{Y}{W} + g\cos\theta\sin\phi - ru + pw, \tag{2.2}$$

$$\dot{w} = g\frac{Z}{W} + g\cos\theta\cos\phi + qu - pv, \tag{2.3}$$

$$\dot{p} = \frac{I_{zz}}{I_D}\left[L + I_{xz}pq - (I_{zz} - I_{yy})\,qr\right] + \frac{I_{xz}}{I_D}\left[N - I_{xz}qr - (I_{yy} - I_{xx})\,pq\right], \tag{2.4}$$

$$\dot{q} = \frac{1}{I_{yy}}\left[M - (I_{xx} - I_{zz})\,pr - I_{xz}\left(p^2 - r^2\right)\right], \tag{2.5}$$

$$\dot{r} = \frac{I_{xz}}{I_D}\left[L + I_{xz}pq - (I_{zz} - I_{yy})\,qr\right] + \frac{I_{xx}}{I_D}\left[N - I_{xz}qr - (I_{yy} - I_{xx})\,pq\right], \tag{2.6}$$

$$\dot{\phi} = p + q\sin\phi\tan\theta + r\cos\phi\tan\theta, \tag{2.7}$$

$$\dot{\theta} = q\cos\phi - r\sin\phi, \tag{2.8}$$

$$\dot{\psi} = (qsin\phi + r\cos\phi)\sec\theta, \tag{2.9}$$

In the above, $I_D = I_{xx}I_{zz} - I_{xz}^2$; X, Y , and Z are the aerodynamic forces in body axes at the nominal CG, and L, M, and N are the aerodynamic moments about the same point. The values of the gross aircraft weight W, the moments of inertia I_{xx}, I_{yy}, and I_{zz}, as well as the product of inertia I_{xz} can be found in [19].

The following navigation equations determine x and y, the positions of the aircraft in the north and east directions respectively, as well as the altitude h:

$$\dot{x} = u\cos\theta\cos\psi + v(-\cos\phi\sin\psi + \sin\phi\sin\theta\cos\psi) + \tag{2.10}$$
$$w(\sin\phi\sin\psi + \cos\phi\sin\theta\cos\psi),$$

$$\dot{y} = u\cos\theta\sin\psi + v(\cos\phi\cos\psi + \sin\phi\sin\theta\sin\psi) + \tag{2.11}$$
$$w(-\sin\phi\cos\psi + \cos\phi\sin\theta\sin\psi),$$

$$\dot{h} = u\sin\theta - v\sin\phi\cos\theta - w\cos\phi\cos\theta. \tag{2.12}$$

It is often convenient to replace the body-fixed velocities with the true airspeed V_T, the angle-of-attack α, and the side-slip angle β. These new states can be calculated

from the body-fixed velocities, neglecting wind and gust-induced effects, as

$$V_T = \sqrt{u^2 + v^2 + w^2}, \tag{2.13}$$

$$\tan\alpha = \frac{w}{u}, \tag{2.14}$$

$$\sin\beta = \frac{v}{V_T}. \tag{2.15}$$

It is well known [21] that the aerodynamic forces and moments acting on the aircraft can be expressed in terms of the non-dimensional force and moment coefficients through multiplication by a denationalizing factor and, in the case of the forces, a transformation from wind to body axes. The forces and moments are therefore given by

$$\begin{bmatrix} X \\ Y \\ Z \end{bmatrix} = \bar{q}S \begin{bmatrix} \cos\alpha & 0 & -\sin\alpha \\ 0 & 1 & 0 \\ \sin\alpha & 0 & \cos\alpha \end{bmatrix} \begin{bmatrix} -C_D \\ C_Y \\ -C_L \end{bmatrix}, \tag{2.16}$$

$$\begin{bmatrix} L \\ M \\ N \end{bmatrix} = \bar{q}S \begin{bmatrix} b_{ref}C_l \\ c_{ref}C_m \\ b_{ref}C_n \end{bmatrix}, \tag{2.17}$$

where C_L, C_D, and C_Y are the lift, drag, and side-force coefficients respectively while C_l, C_m, and C_n are the moment coefficients. The values of the the wingspan b_{ref}, the mean aerodynamic chord c_{ref}, and the wing surface area S can be found in [19].

Table 2.1 shows the aircraft states, plant (i.e., inputs to the plant), control (i.e., outputs of the controller), and pilot inputs. The system state vector is given by

$$X = [V_T \quad \alpha \quad \beta \quad p \quad q \quad r \quad \phi \quad \theta \quad \psi \quad x \quad y \quad h]^T. \tag{2.18}$$

The pilot inputs are ailerons, rudders, and elevators commands. Plant inputs are 4 engine throttles and the deflection of 6 control surfaces. As in the early version of the GTM the engines are not controllable. Therefore, the throttle values will be fixed at their trim values except for in Chapter 6.

Table 2.1: Aircraft states, actuators, and pilot inputs.

Variable	Description	Component of
V_t	Velocity	State (x)
α	Angle of Attack	State (x)
β	Side-slip Angle	State (x)
ϕ	Euler Angle	State (x)
θ	Euler Angle	State (x)
ψ	Euler Angle	State (x)
p	Roll Rate	State (x)
q	Pitch Rate	State (x)
r	Yaw Rate	State (x)
t_1	Left outboard Throttle	Plant input
t_2	Left Inboard Throttle	Plant input
t_3	Right Inboard Throttle	Plant input
t_4	Right outboard Throttle	Plant input
e_1	Left Elevator	Plant input, Control output (u)
e_2	Right Elevator	Plant input, Control output (u)
a_1	Left Aileron	Plant input, Control output (u)
a_2	Right Aileron	Plant input, Control output (u)
r_1	Lower Rudder	Plant input, Control output (u)
r_2	Upper Rudder	Plant input, Control output (u)
$\delta_{\text{e,cmd}}$	Virtual Elevator	Pilot input (r)
$\delta_{\text{a,cmd}}$	Virtual Aileron	Pilot input (r)
$\delta_{\text{r,cmd}}$	Virtual Rudder	Pilot input (r)

The virtual inputs available to the pilot are the elevator, aileron, and rudder commands denoted as $\Delta\delta_{\mathrm{e,cmd}}$, $\Delta\delta_{\mathrm{a,cmd}}$, and $\Delta\delta_{\mathrm{r,cmd}}$. The aerodynamic force and moment coefficients are given by

$$\begin{aligned}
C_L &= C_{L_\alpha}\alpha + C_{L_{\delta_e}}\delta_e, \\
C_D &= C_{D_\alpha}\alpha + C_{D_{\delta_e}}\delta_e, \\
C_Y &= C_{Y_\beta}\beta + C_{Y_p}p\frac{b_{ref}}{2V_T} + (C_{Y_r} - C_{Y_{\dot\beta}})(r-\dot\beta)\frac{b_{ref}}{2V_T} + C_{Y_{\delta_a}}\delta_a + C_{Y_{\delta_r}}\delta_r,
\end{aligned} \tag{2.19}$$

$$\begin{aligned}
C_l &= C_{l_\beta}\beta + C_{l_p}p\frac{b_{ref}}{2V_T} + (C_{l_r} - C_{l_{\dot\beta}})(r-\dot\beta)\frac{b_{ref}}{2V_T} + C_{l_{\delta_a}}\delta_a + C_{l_{\delta_r}}\delta_r, \\
C_m &= C_{m_{alpha}}\alpha + (C_{m_q} + C_{m_{\dot\alpha}})(q-\dot\alpha)\frac{c_{ref}}{2V_T} + C_{m_{\delta_e}}\delta_e, \\
C_n &= C_{n_\beta}\beta + C_{n_p}p\frac{b_{ref}}{2V_T} + (C_{n_r} - C_{n_{\dot\beta}})(r-\dot\beta)\frac{b_{ref}}{2V_T} + C_{n_{\delta_a}}\delta_a + C_{n_{\delta_r}}\delta_r,
\end{aligned} \tag{2.20}$$

where

$$\begin{aligned}
\delta_e &= \frac{e_1 + e_2}{2}, \\
\delta_a &= \frac{a_1 - a_2}{2}, \\
\delta_r &= \frac{r_1 + r_2}{2}.
\end{aligned} \tag{2.21}$$

These set of equations prescribe the non-dimensional coefficients in Equations (2.16) and (2.17) as a a function of the state. In the context of Chapters 2-5, the control surface deflections are related to the control inputs by $u_1 = e_1$, $u_2 = e_2$, $u_3 = a_1$, $u_4 = a_2$, $u_5 = r_1$, and $u_6 = r_2$. Overall, the aircraft dynamics is given by the equations above along with an aerodynamic model. The model to be used herein is prescribed subsequently.

We can compactly describe the overall nonlinear model as

$$\dot X = F(X, \Lambda U) \tag{2.22}$$

where the input U consists of u_i, for $i = 1,..6$, and Λ is the control effectiveness

matrix.

For control purposes, the nonlinear plant is linearized about a trim point (X_0, U_0) satisfying $F(X_0, U_0) = 0$. This leads to the linear time invariant system

$$\dot{x_p} = A_p x_p + B_p u + g(x_p, u) \tag{2.23}$$

where

$$A_p = \left.\frac{\partial F(X,U)}{\partial X}\right|_{X_0,\, U_0}, \quad B_p = \left.\frac{\partial F(X,U)}{\partial U}\right|_{X_0,\, U_0}, \tag{2.24}$$

and $g(x_p, u)$ is higher order terms.

2.2 Adverse Conditions

We now describe the three categories of upsets, damages, and failures that we shall introduce in the above model.

2.2.1 Flight upsets:

These adverse conditions result from large deviations in the initial conditions of the state from its trim value. If a system is stable, guarantees for a bounded performance are automatically obtained. Since in practical situations the closed-loop system is subject to unknown bounded disturbances, case for which only uniform ultimate boundedness can be proved, there are initial conditions for which the state may grow unbounded. Whether the actual responses are bounded and actually stay within limits of what is an acceptable remains to be demonstrated. In this paper, $\alpha(0)$ will be considered as an uncertain parameter. Since the baseline controller designed for the GTM does not enable lateral command following, flight upsets in $\beta(0)$ were not studied.

2.2.2 CG movement:

A serious condition that needs to be addressed is structural damage. This causes, among other things, a movement of the CG from its nominal position. Assuming that this movement only occurs in the xy plane, the changes to Equation (2.17) are given by

$$\begin{aligned} \Delta L &= (Lcos\alpha + Dsin\alpha)\Delta y \\ \Delta M &= -(Lcos\alpha + Dsin\alpha)\Delta x \\ \Delta N &= (Dcos\alpha - Lsin\alpha)\Delta y \end{aligned} \tag{2.25}$$

where Δx and Δy is the displacement from the nominal CG location to the post-failure one. The contribution of the tangential component of the acceleration can be accounted for by using the inertia tensor about the actual CG

$$\begin{aligned} I'_{xx} &= I_{xx} + m\Delta y^2 \\ I'_{yy} &= I_{yy} + m\Delta x^2 \\ I'_{zz} &= I_{zz} + m\Delta x^2 + m\Delta y^2 \end{aligned} \tag{2.26}$$

In the studies that follow the contribution of the centripetal component of the acceleration resulting from CG movement is ignored. The reader can refer to [15] for an explicit formulation of the equations of motion.

2.2.3 Actuator Failures:

We now consider adverse conditions that result from losses in control effectiveness and time delay.

As in reference [22], we model these failures by pre-multiplying the B_p matrix of the linearized model by the control effectiveness matrix Λ. That is, the B_p matrix in (2.23) is changed to $B_p\Lambda$ where Λ is a matrix of dimension 6×6, which is equal to the identity matrix in the nominal case. Losses in control effectiveness are modeled by making the terms in the diagonal of Λ to assume values between zero and one.

For example, if the right elevator fails by 50%, and the left aileron fails by 40%, Λ takes on the form

$$\Lambda = \text{diag}\begin{bmatrix} 1 & 0.5 & 0.6 & 1 & 1 & 1 \end{bmatrix}.$$

In general, the control effectiveness matrix takes the form

$$\Lambda = \text{diag}\begin{bmatrix} \lambda_{e1} & \lambda_{e2} & \lambda_{a1} & \lambda_{a2} & \lambda_{r1} & \lambda_{r2} \end{bmatrix}, \tag{2.27}$$

where $0 \leq \max\{\Lambda\} \leq 1$.

In addition to these actuator failures we will also consider time delay in all six control inputs and control surface lock-ups. In the latter type, the uncertain parameter is the duration of the lock-on-place failure. Note that from all uncertainties mentioned above, only those in Λ affect the value of the control U_0 at trim.

Chapter 3

Adaptive Control Architecture

The control architecture proposed augments a nominal controller with an adaptive component. While the nominal controller is designed to meet the performance requirements under ideal operating conditions, the adaptive one copes with failures and uncertainties. The very same structure of the controller that Langley designed for the GTM will be used in the nominal controller. Details on such a structure are presented next.

3.1 Nominal Controller

The nominal controller has three main components, an array of low-pass and wash-out and filters, an LQR controller with integral action, and a hard-limiter to cope with control saturation. This limiter enforces an anti-integration windup logic based on the elevator deflection. This logic makes the system linear time varying. Each of these components is described in more detail next.

3.1.1 Washout Filters and Low-pass Filters

The GTM model has an array of low-pass and wash-out and filters to mitigate measurement noise and improve handling qualities. A block diagram of the system is shown in Figure 3-1. In particular, the states α, p, q, and r will be low-pass filtered

but only p, q, and r will be washed-out. These filters will be taken into account when designing the nominal controller.

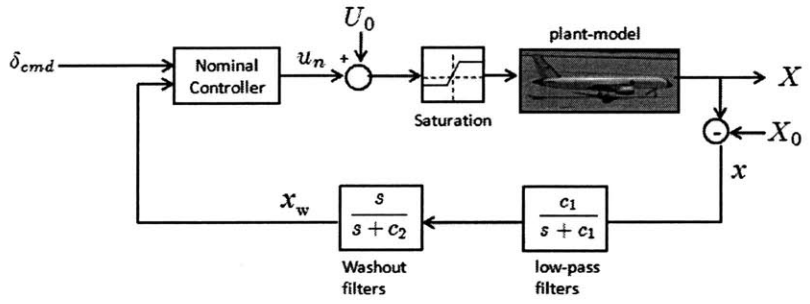

Figure 3-1: Washout filters and low-pass filters

3.1.2 LQR Controller with Integral Action

For control design purposes, we assume that the pitch, yaw and roll dynamics are weakly coupled. In order to closely follow a command in angle of attack, an integral state e_α is added

$$e_\alpha = \int(\alpha - \alpha_{\text{cmd}})dt \tag{3.1}$$

where $\alpha_{\text{cmd}} = 10\delta_{\text{e,cmd}}$. Note that elevator command does not affect elevator angle, instead it generates integral error. The signal $\delta_{\text{e,cmd}}$ is one of the plant inputs in $\delta_{\text{cmd}} = \begin{bmatrix}\delta_{\text{e,cmd}} & \delta_{\text{a,cmd}} & \delta_{\text{r,cmd}}\end{bmatrix}^T$. The augmented plant dynamics is therefore described as

$$\underbrace{\begin{bmatrix}\dot{x}_p \\ \dot{e}_\alpha\end{bmatrix}}_{\dot{x}} = \underbrace{\begin{bmatrix}A_p & 0 \\ H & 0\end{bmatrix}}_{A}\underbrace{\begin{bmatrix}x_p \\ e_\alpha\end{bmatrix}}_{x} + \underbrace{\begin{bmatrix}B_p \\ 0\end{bmatrix}}_{B_1} u + \underbrace{\begin{bmatrix}0 \\ -I\end{bmatrix}}_{B_2}\alpha_{\text{cmd}} \tag{3.2}$$

Since the states in Equation (3.2) are accessible, an LQR controller is designed as

$$\begin{aligned} \delta_{e,n} &= -\begin{bmatrix} K_{\delta_{e\alpha}} & K_{\delta_{eq}} & K_{\delta_{ee}} \end{bmatrix} \begin{bmatrix} \alpha \\ q \\ e_\alpha \end{bmatrix} \\ \begin{bmatrix} \delta_{a,n} \\ \delta_{r,n} \end{bmatrix} &= -\begin{bmatrix} K_{\delta_{ap}} & 0 \\ 0 & K_{\delta_{rr}} \end{bmatrix} \begin{bmatrix} p \\ r \end{bmatrix} + \underbrace{\begin{bmatrix} \delta_{a,cmd} \\ \delta_{r,cmd} \end{bmatrix}}_{K_r \delta_{\text{cmd}}} \end{aligned} \tag{3.3}$$

where the control gains K_δ minimize the cost function

$$J = \int (x^T R_{xx} x + u^T R_{uu} u) dt, \tag{3.4}$$

and R_{xx}, R_{uu} are weighting matrices. When only the baseline controller is used $u = u_n = [\delta_{e,n}, \delta_{a,n}, \delta_{e,n}]$ and that $e_1 = e_2 = \delta_{e,n}/2$, $a_1 = -a_2 = \delta_{a,n}/2$ and $r_1 = r_2 = \delta_{r,n}/2$. Equations (3.1)-(3.3) prescribe the closed-loop dynamics of an LTI approximation of the GTM for an LQR controller with integral action.

3.2 Saturation

To ensure that the control input does not exceed the saturation limits for the three control surfaces, the rectangular saturation function

$$R_s(u_i) = \begin{cases} u_i & \text{if } \|u_i\| \leq u_{i,max}, \\ u_{i,max}\ \text{sign}(u_i) & \text{if } \|u_i\| > u_{i,max}, \end{cases} \tag{3.5}$$

is used. The control deficiency caused by saturation is given by

$$u_\Delta = u - R_s(u). \tag{3.6}$$

Besides this physical saturation constraint, an anti-windup logic that depends on

e_α is also implemented. This logic is governed by the time-varying saturation function

$$R_e(e_\alpha, \delta_e(t)) = \begin{cases} e_\alpha & \text{if } \dot{e}_\alpha \geq 0 \text{ or } e_\alpha \leq e_{\text{available}}, \\ e_{\text{available}} & \text{if } \dot{e}_\alpha < 0 \text{ and } e_\alpha > e_{\text{available}}. \end{cases} \tag{3.7}$$

where $e_{\text{available}}$ is given by

$$e_{\text{available}} = \max\left\{0, \frac{R_s(\delta_e) - (\delta_{e,\text{trim}} + K_{\delta_{e_\alpha}}\alpha + K_{\delta_{e_q}} q_w)}{K_{\delta_{e_\alpha}}}\right\}. \tag{3.8}$$

The error deficiency caused by the saturation function in Equation (3.7) is defined as

$$e_{\alpha,\Delta} = e_\alpha - R_e(e_\alpha, \delta_e(t)). \tag{3.9}$$

By replacing u with $R_s(u_n)$, and e_α with $R_e(e_\alpha, \delta_e(t))$ in Equation (3.2) we obtain the LTV system

$$\begin{aligned} \underbrace{\begin{bmatrix} \dot{x}_p \\ \dot{e}_\alpha \end{bmatrix}}_{\dot{x}} &= \underbrace{\begin{bmatrix} A_p - B_p K_{x_p} & -B_p K_{\delta_{e_\alpha}} \\ H & 0 \end{bmatrix}}_{A_m} \underbrace{\begin{bmatrix} x_p \\ e_\alpha \end{bmatrix}}_{x} + \underbrace{\begin{bmatrix} B_p \\ 0 \end{bmatrix}}_{B_1} K_r \delta_{cmd} \\ &+ \underbrace{\begin{bmatrix} 0 \\ -I \end{bmatrix}}_{B_2} \alpha_{cmd} - \underbrace{\begin{bmatrix} B_p \\ 0 \end{bmatrix}}_{R_1} u_\Delta - \underbrace{\begin{bmatrix} -B_p K_{\delta_{e_\alpha}} \\ 0 \end{bmatrix}}_{R_2} e_{\alpha,\Delta}, \end{aligned} \tag{3.10}$$

which is the closed-loop system corresponding to the nominal controller. The boundedness of this system can be established for all initial conditions inside a bounded set. This bounded set extends to the entire state-space when the open-loop plant is stable and there is no unmodeled dynamics (e.g., time-delay).

3.3 Adaptive Controller

Since the nominal controller in (3.3) has been designed for a plant-model under nominal conditions, it may prove to be inadequate in the face of failures and uncertainties.

To mend for this we augment the controller in (3.3) with an adaptive component as follows:

$$u = U_0 + u_n + u_a = U_0 + (K + \theta_x)x + (K_r + \theta_r)r + \hat{f} \tag{3.11}$$

where θ_x, θ_r, and $\hat{f}$ are adjusted to minimize the state error between the controlled plant-model and a reference model. The latter is chosen to generate the desired plant output for the commanded input. In the current problem, the reference model is given by the non-linear closed-loop system corresponding to the baseline controller for the case where there are no uncertainties. Besides, none of the saturation functions above are part of the reference model. Figure 3-2 shows the block diagram of this control architecture. Adaptive controllers for the GTM using a reference model that

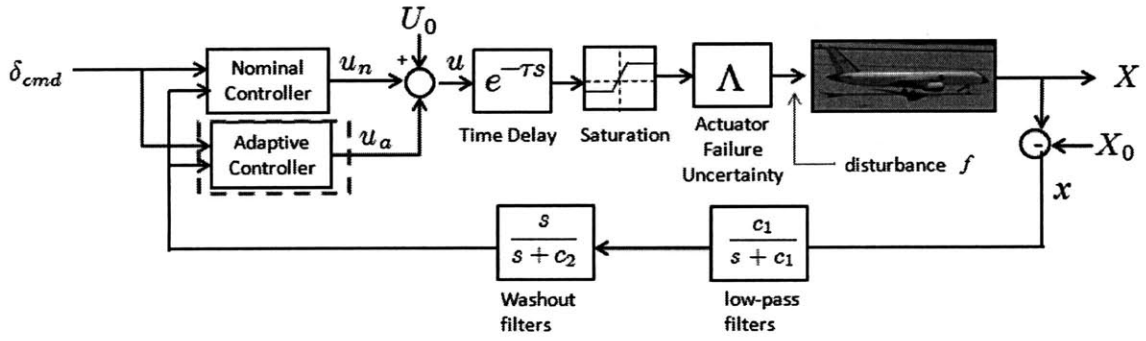

Figure 3-2: Control Architecture.

accounts for the time delay in telemetry have shown promise. Such controllers will be presented in Chapter 6.

Let x_m be the state of the reference model. Defining the state error e as

$$e = x - x_m \tag{3.12}$$

we choose the adaptive laws for adjusting the adaptive parameters in (3.11) as

$$\begin{aligned}
\dot{\theta}_x &= -\Gamma_1 B^T P e_u x^T - \sigma_1 \theta_x \\
\dot{\theta}_r &= -\Gamma_2 B^T P e_u r - \sigma_2 \theta_r \\
\dot{\hat{f}} &= -\Gamma_3 B^T P e_u - \sigma_3 \theta_f \\
\dot{\hat{\lambda}} &= -\Gamma_4 \mathrm{diag}(u_\Delta) B_p^T P e_u - \sigma_4 \hat{\lambda}
\end{aligned} \tag{3.13}$$

where $A_m^T P + P A_m = -Q$, $Q > 0$, Γ_i is diagonal and positive definite for $i = 1, ...4$, and $e_u = e - e_\Delta$. The auxiliary error e_Δ is defined as

$$\dot{e}_\Delta = A_m e_\Delta - R_1 \mathrm{diag}(\hat{\lambda}) u_\Delta. \tag{3.14}$$

Note that if the control does not saturate $u_\Delta = 0$, $e_\Delta \to 0$ and $e_u \to e$. e_Δ is the error that occurs due to saturation, and by subtracting it out from e, we obtain e_u which is the sum of the error due to uncertainties and the error due to $e_{\alpha,\Delta}$. The σ modifications prevent the drift of the adaptive parameters θ_x, θ_r, $\hat{f}$ and $\hat{\lambda}$ caused by disturbances. The term $\hat{f}$ is an adaptive parameter aimed at counteracting constant disturbances.

It should be noted that the stability and boundedness of the closed-loop augmented system has been proved in [7, 11, 23] when physical saturation constraints are present. The stability analysis for the resetting-based anti-windup logic was also established and to be appeared elsewhere.

Chapter 4

Control Verification

This chapter introduces a framework for evaluating the degradation in closed-loop performance caused by increasingly larger values of uncertainty. This is attained by determining the largest hyper-rectangular set in the uncertain parameter space for which a set of closed-loop requirements are satisfied by all set members. A brief introduction to the mathematical framework required to perform this study is presented next. References [16] and [18] cover this material in more detail.

4.1 Mathematical Framework

The parameters which specify the closed-loop system are grouped into two categories: uncertain parameters, which are denoted by the vector p, and the control design parameters, which are denoted by the vector d. While the plant model depends on p (e.g., aerodynamic coefficients, initial conditions, time delay, actuator failures), the controller depends on d (e.g., control gains). The *Nominal Parameter* value, denoted as $\bar{p}$, is the value that p assumes when there is no failure/uncertainty. The value of d on the other hand is assumed to be available and will remain fixed.

Stability and performance requirements for the closed-loop system will be prescribed by the set of constraint functions, $g(p, d) < 0$. This vector inequality, as all others that follow, hold component wise. For a fixed d, the larger the region in p-space where $g < 0$, the more robust the controller. The *Failure Domain* corresponding to

the controller with parameters d is given by[1]

$$\mathcal{F}(d) = \bigcup_{j=1}^{\dim(g)} \mathcal{F}^j(d). \tag{4.1}$$

$$\mathcal{F}^j(d) = \{p : g_j(p,d) \geq 0\}, \tag{4.2}$$

While Equation (4.2) describes the failure domain corresponding to the jth requirement, Equation (4.1) describes the failure domain for all requirements. The *Non-Failure Domain* is the complement set of the failure domain and will be denoted[2] as $C(\mathcal{F})$. The names "failure domain" and "non-failure domain" are used because in the failure domain at least one constraint is violated while, in the non-failure domain, all constraints are satisfied.

Let Ω be a set in p-space, called the *Reference Set*, whose geometric center is the nominal parameter $\bar{p}$. The geometry of Ω will be prescribed according to the relative levels of uncertainty in p. One possible choice for the reference set is the hyper-rectangle

$$\mathcal{R}(\bar{p}, n) = \{p : \bar{p} - n \leq \ p \leq \bar{p} + n\}. \tag{4.3}$$

where $n > 0$ is the vector of half-lengths. One of the tasks of interest is to assign a measure of robustness to a controller based on measuring how much the reference set can be deformed before intersecting the failure domain. The *Homothetic Deformation* of Ω with respect to the nominal parameter point $\bar{p}$ by a factor of $\alpha \geq 0$, is the set $\mathcal{H}(\Omega, \alpha) = \{\bar{p} + \alpha(p - \bar{p}) : p \in \Omega\}$. The factor of this deformation, α, is called the *Similitude Ratio*. While expansions are accomplished when $\alpha > 1$, contractions result when $0 \leq \alpha < 1$. Hereafter, deformations must be interpreted as homothetic expansions or contractions.

In what follows we assume that the controller d satisfies the requirements for the nominal plant, i.e., $g(\bar{p}, d) < 0$. Intuitively, one imagines that a homothet of the reference set is being deformed until its boundary touches the failure domain. Any

[1]Throughout this thesis, super-indices are used to denote a particular vector or set while sub-indices refer to vector components, e.g., p_i^j is the ith component of the vector p^j.

[2]The complement set operator will be denoted as $C(\cdot)$.

point where the deforming set touches the failure domain is a *Critical Parameter Value* (CPV). The CPV, which will be denoted as $\tilde{p}$, might not be unique. The deformed set is called the *Maximal Set* (MS) and will be denoted as $\mathcal{M}$. The MS is the largest homothet of Ω that fits within $C(\mathcal{F})$. The *Critical Similitude Ratio* (CSR), denoted as $\tilde{\alpha}$, is the similitude ratio of that deformation. While the CSR is a non-dimensional number, the *Parametric Safety Margin* (PSM), denoted as ρ and defined later, is its dimensional equivalent. Both the CSR and the PSM quantify the size of the MS. Details on the implementation of these ideas are presented next.

The CPV corresponding to the deformation of $\Omega = \mathcal{R}(\bar{p}, n)$ for the jth requirement is given by

$$\tilde{p}^j = \arg\min_p \left\{ \|p - \bar{p}\|_n^\infty : g_j(p, d) \geq 0, Ap \geq b \right\}, \tag{4.4}$$

where $\|x\|_n^\infty = \sup_i\{|x_i|/n_i\}$ is the n-scaled infinity norm. The last constraint in Equation (4.4) is used to exclude regions of the parameter space where plants are infeasible and uncertainty levels are unrealistic. The overall CPV is

$$\tilde{p} = \tilde{p}^k, \tag{4.5}$$

where

$$k = \arg\min_{1 \leq j \leq \dim(g)} \left\{ \|\tilde{p}^j - \bar{p}\|_n^\infty \right\}. \tag{4.6}$$

The critical requirement, which is the one preventing a larger deformation, is $g_k < 0$. Once the CPV has been found, the MS is uniquely determined by

$$\mathcal{M}(d) = \mathcal{R}(\bar{p}, \tilde{\alpha} n). \tag{4.7}$$

where $\tilde{\alpha} = \|\tilde{p} - \bar{p}\|_n^\infty$. The *Rectangular PSM* is defined as

$$\rho = \tilde{\alpha} \|n\|, \tag{4.8}$$

The last two equations, which apply to the overall CPV, can be extended to individual CPVs, by using $\tilde{p}^j$ instead of $\tilde{p}$. Note that overall PSM is equal to the smallest

individual PSM.

Because the CSR and the PSM measure the size of the MS, their values are proportional to the degree of robustness of the controller associated with d to uncertainty in p. The CSR is non-dimensional, but depends on both the shape and the size of the reference set. The PSM has the same units as the uncertain parameters, and depends on the shape, but not the size, of the reference set. If the PSM is zero, the controller's robustness is practically nil since there are infinitely small perturbations of $\bar{p}$ leading to the violation of at least one of the requirements. If the PSM is positive, the requirements are satisfied for parameter points in the vicinity of the nominal parameter point. The larger the PSM, the larger the Ω-shaped vicinity.

4.1.1 One-dimensional Case

In the case where $\dim\{p\} = 1$, the expressions for the CPVs, the PSM, and the MS are given by

$$\tilde{p}^j = \arg\min_p \{|p - \bar{p}| : g_j(p, d) \geq 0, Ap \geq b\}, \tag{4.9}$$

$$\tilde{p} = \tilde{p}^k, \tag{4.10}$$

$$\rho = |\tilde{p}^k - \bar{p}|, \tag{4.11}$$

$$\mathcal{M}(d) = (\bar{p} - \rho, \bar{p} + \rho), \tag{4.12}$$

where

$$k = \arg \min_{1 \leq j \leq \dim(g)} \left\{|\tilde{p}^j - \bar{p}|\right\}. \tag{4.13}$$

Figure 4-1 shows an sketch with relevant variables and sets. Note that the non-failure domain is given by the intersection of the individual non-failure domains. Besides, the overall CPV is the parameter value closest to the nominal point where at least one component of g is equal to zero. From the figure we see that $\tilde{p}^1 - \bar{p} < \bar{p} - \tilde{p}^2$ so $\tilde{p} = \tilde{p}^1$ and $k = 1$. By construction, all the points within the MS, which is centered about the nominal parameter point, satisfy the closed-loop requirements.

As expected, analyzes arising from considering each uncertain parameter individu-

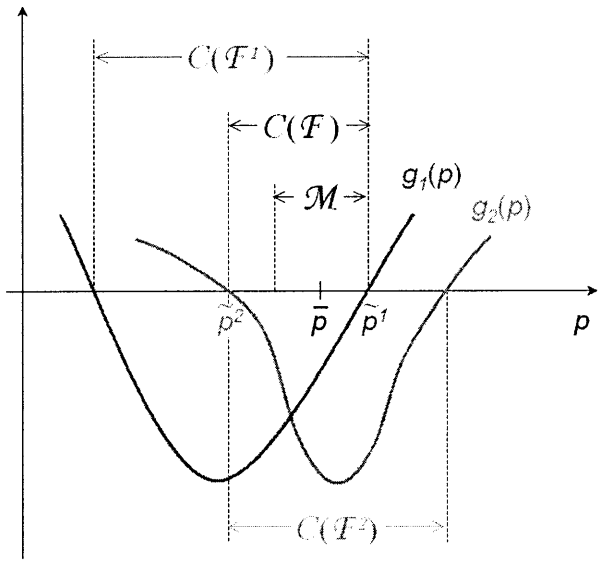

Figure 4-1: Relevant variables in the 1-dimensional parameter space.

ally are unable to capture the effect of the dependencies among uncertain parameters. When such dependencies are important, the collection of PSMs that result from performing $\dim(p)$ one-dimensional deformations can misrepresent the actual system's robustness. For instance, if ρ^1 is the PSM corresponding to a one-dimensional deformation in p_1, ρ^2 is the PSM corresponding to a one-dimensional deformation in p_2, and ρ^3 is the PSM corresponding to a two-dimensional deformation in $[p_1, p_2]$; it is possible to have $\rho^3 \ll \min\{\rho^1, \rho^2\}$. In such a case there is a combination of uncertain parameters much closer to $\bar{p}$ that will be missed by both one-dimensional searches.

4.2 Analysis Setup

4.2.1 Uncertain Parameters

We will consider the following set of uncertain parameters

$$[\Lambda_{\text{ele}}, \Lambda_{\text{ail}}, \Lambda_{\text{rud}}, \Lambda_{\text{thr}}, \tau, t_l, \Delta_x, \Delta_y, \Delta\alpha(0)], \tag{4.14}$$

where the first 6 components, can be categorized as actuator uncertainties or failures, the next two account for structural failures and last one for a flight upset. In particular,

$$\begin{aligned}\Lambda_{\text{ele}} &= \left[\lambda_{e1}, \lambda_{e2}\right] \\ \Lambda_{\text{ail}} &= \left[\lambda_{a1}, \lambda_{a2}\right] \\ \Lambda_{\text{rud}} &= \left[\lambda_{r1}, \lambda_{r2}\right] \\ \Lambda_{\text{thr}} &= \left[\lambda_{t1}, \lambda_{t2}, \lambda_{t3}, \lambda_{t4}\right]\end{aligned} \tag{4.15}$$

are the control effectiveness of elevators, ailerons, rudders, and engine throttle; τ is a time delay in all input channels, and t_l is the duration of a control surface lock-up. The terms Δ_x and Δ_y are components of the position vector in the xy-body frame of the post-failure CG location with respect to a reference point. The last component, which models a flight upset, is the initial condition in angle of attack. The nominal parameter values corresponding to the set of parameters in Equation (4.14) is $[1, 1, 1, 1, 0, 0, 0, 0, 0, 0]$.

4.2.2 Closed-loop Requirements

The following stability and performance requirements will be considered

$$g_0 = \max\{[u_{trim} - u_{\max}, u_{\min} - u_{trim}]\}, \tag{4.16}$$

$$g_1 = \max_t \left\{ \frac{|\dot{V}_T|}{g} \right\} - 2.5, \tag{4.17}$$

$$g_2 = \left[(\alpha - \alpha_{\text{cmd}})^2 + k_\alpha \dot{\alpha}^2 + (\beta - \beta_{\text{cmd}})^2 + k_\beta \dot{\beta}^2\right]_{t=t_f} - c_1, \tag{4.18}$$

$$
\begin{aligned}
g_3 &= \eta(p,d) - c_2\eta(\bar{p}, d_{base}), \\
\eta &= w_1||\alpha - \alpha_{\text{cmd}}||_2 + w_2||p - p_{\text{cmd}}||_2 + w_3||r - r_{\text{cmd}}||_2.
\end{aligned}
\tag{4.19}
$$

The first requirement, $g_0 < 0$, is used to determine if the vehicle has enough control authority to trim, i.e. if it satisfies $u_{min} < u_{trim} < u_{max}$. Note that this requirement is independent of d and may indicate instability. $g_1 < 0$ is a structural requirement enforced by preventing the loading factor from exceeding the upper limit of 2.5. The requirement $g_2 < 0$, where $0 < c_1 \ll 1$, $k_\alpha > 0$ and $k_\beta > 0$, enforces stability and satisfactory steady state performance. The last requirement, $g_3 < 0$, for $c_2 > 1$, $w_1 > 0$, $w_2 > 0$ and $w_3 > 0$, is used to measure satisfactory transient performance. This requirement prevents the cumulative error from exceeding a prescribed upper limit. Such a limit is c_2 times larger than the cumulative error incurred by the baseline controller under nominal flying conditions.

In practice, control requirements are prescribed in advance before the control design process even starts. When such requirements are only described qualitatively several g implementations are possible. This creates the additional challenge of constructing functional forms that capture well the intent of the requirement while having a minimal amount of conservatism. This thesis does not tackle such a challenge and assumes that the g above is given.

4.3 Flight Conditions (FC)

The closed-loop response depends on p and d as well as on the intended flight maneuver f. This implies that $g(p,d,f)$. Two flight conditions, namely f_{lon} and f_{lat}, will be considered in the analyzes that follow. In the former one, which mostly affects the longitudinal dynamics, a step input in $\delta_{e,cmd}$ is commanded. In the second one, which affects both the longitudinal and lateral dynamics, the vehicle also starts from level flight and a set of commands in $\delta_{a,cmd}$ and $\delta_{r,cmd}$ makes the vehicle turn. Figures 4-2 and 4-3 show the vehicle's trajectory as well as relevant states for both flight conditions when there is no uncertainty/failure. The p command for f_{lat} is a

sequence of two step inputs (only one is shown) where the second one is commanded so that it cancels the first one after a suitable time.

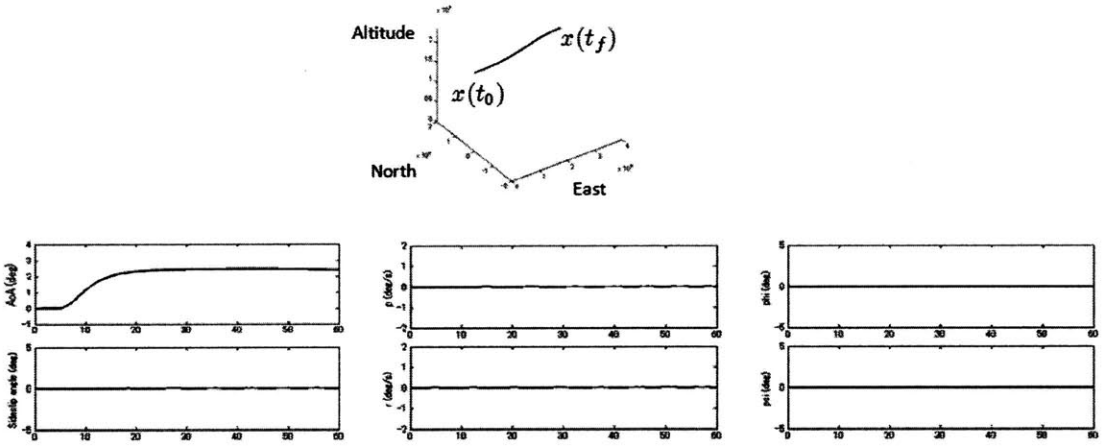

Figure 4-2: Time simulation for the longitudinal flight condition.

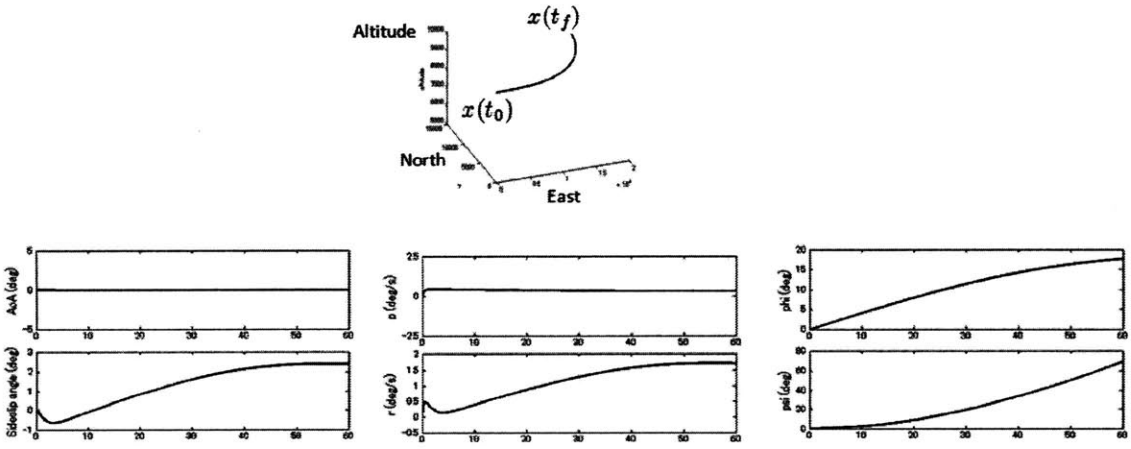

Figure 4-3: Time simulation for lateral flight condition.

Chapter 5

Results

In this chapter, we evaluate the baseline controller in Equation (3.10) and the adaptive controller in Equations (3.11) - (3.14) according to the control verification setting of Chapter 4. The aerodynamic model used can be found in [19]. The numerical value of other variables are shown in Table 5.2.

5.1 One-dimensional Case

In Case A we consider a flight upset in the angle of attack, $\Delta\alpha(0)$ about $\alpha_{\text{trim}} = 2.20(\text{deg})$ for the longitudinal flight condition. The dependency of g on $\Delta\alpha(0)$ for both controllers is illustrated in Figure 5-1. The dashed lines and the solid lines represent results from the baseline and adaptive controllers respectively. A comparison of these curves shows that the non-failure region of the adaptive controller is larger by virtue of the structural and tracking performance requirements. The same line convention used in this figure applies to those that follow.

In Case B we consider the movement of the CG in the x-direction for the longitudinal flight condition. Recall that a positive value of the CG movement denotes a forward movement. Figure 5-2 illustrates the dependency of g on the CG location for both controllers. Note that the system loses stability when the CG moves backward, while the tracking performance degrades the faster when the CG moves forward. The baseline controller has a PSM of 0.175 while the adaptive one attains a PSM of 0.197.

Table 5.1: Cases analyzed

Case	**Failure/Uncertainty**	
Case A	Flight upset in angle of attack	$[\Delta\alpha(0)\ f_{\text{lon}}]$
Case B	CG movement along x-axis	$[\Delta_x\ f_{\text{lon}}]$
Case C	CG movement along y-axis	$[\Delta_y\ f_{\text{lat}}]$
Case D	Symmetric Aileron failure	$[\Lambda_{\text{ail}}\ f_{\text{lat}}]$
Case E	Symmetric Elevator failure	$[\Lambda_{\text{ele}}\ f_{\text{lon}}]$
Case F	Asymmetric Aileron failure	$[\lambda_{\text{a1}}\ f_{\text{lat}}]$
Case G	Asymmetric Throttle failure	$[\lambda_{\text{t1}}\ f_{\text{lon}}]$
Case H	Elevator lock-in-place failure	$[t_l\ f_{\text{lon}}]$
Case I	Time delay in all control inputs	$[\tau\ f_{\text{lon}}]$

Table 5.2: Numerical Values

Variable	**Value**
Velocity at trim	614(ft/sec)
Angle of Attack at trim	2.2(deg)
Height at trim	20000(ft)
$K_{\delta_{e_\alpha}}$	-0.4420
$K_{\delta_{e_q}}$	-0.9105
$K_{\delta_{e_e}}$	-0.7906
$K_{\delta_{a_p}}$	-0.1000
$K_{\delta_{r_r}}$	-0.3000
Γ_1	$\text{diag}([1,1,100,100,100,100]) \times 200$
Γ_2	$\text{diag}([1,1,100,100,100,100]) \times 100$
Γ_3	$\text{diag}([1,1,100,100,100,100]) \times 50$
Γ_4	$\text{diag}([1,1,1,1,1,1]) \times 100$
Q	$\text{diag}([1,1,1,1,1])$

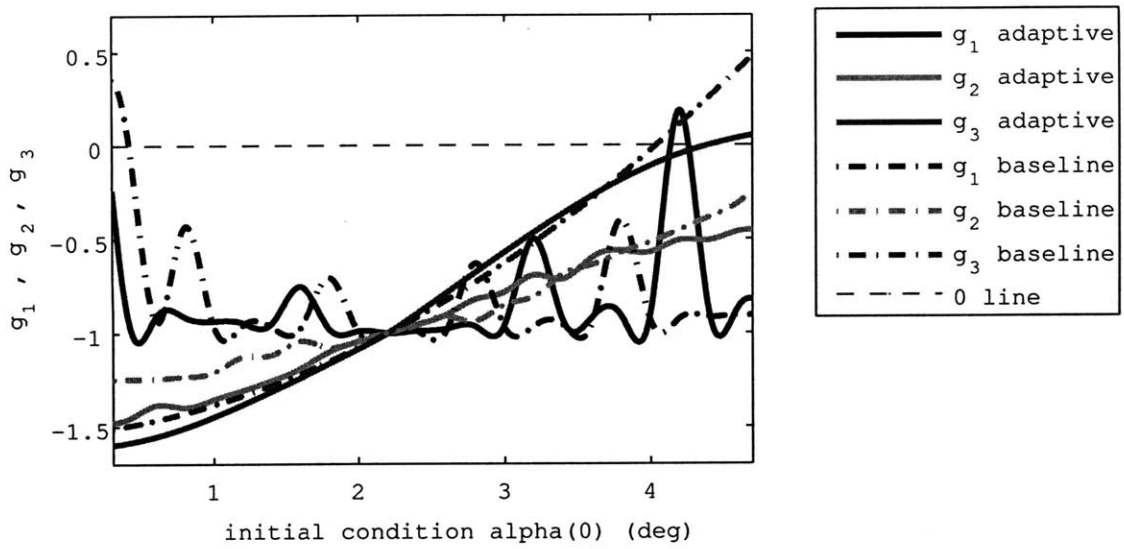

Figure 5-1: Case A: $g(\Delta\alpha(0))$ for the longitudinal FC.

In Case C we consider the movement of the CG in the y-direction for the lateral flight condition. In this setting a positive CG movement denotes a movement to the right. Figure 5-3 illustrates the dependency of g on the CG location for both controllers. The curves are asymmetric with respect to the nominal parameter value, since the flight condition is itself asymmetric. As before, the adaptive controller attains a larger PSM. The baseline controller has a PSM of 0.0029 while the adaptive one attains a PSM of 0.0069.

In Case D, we consider a symmetric failure in both ailerons, where $\lambda_{ail} = \lambda_{a_1} = \lambda_{a_2}$, for the lateral flight condition. Figure 5-4 illustrates the dependency of g on λ_{ail} for both controllers. As before, the adaptive controller attains a larger PSM. While the PSM for the baseline is 6.6%, the PSM for the adaptive is 10%. In both cases, the tracking performance is the critical requirement.

In Case E we consider a symmetric failure in both elevators, where $\lambda_{ele} = \lambda_{e_1} = \lambda_{e_2}$, for the longitudinal flight condition. Figure 5-5 illustrates the dependency of g on λ_{ele} for both controllers. While the PSM for the baseline is 33%, the PSM for the adaptive is 42%. In both cases, the tracking performance is the critical requirement.

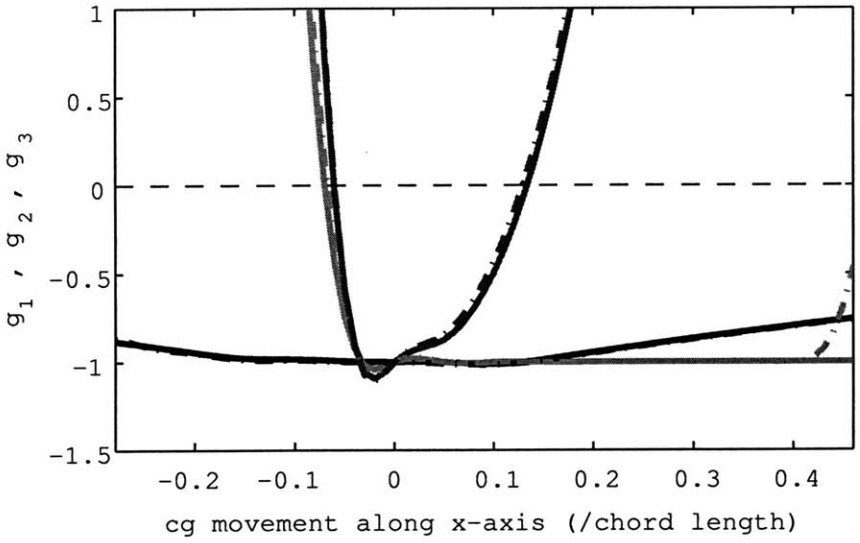

Figure 5-2: Case B: $g(\Delta_x/c_{ref})$ for the longitudinal FC.

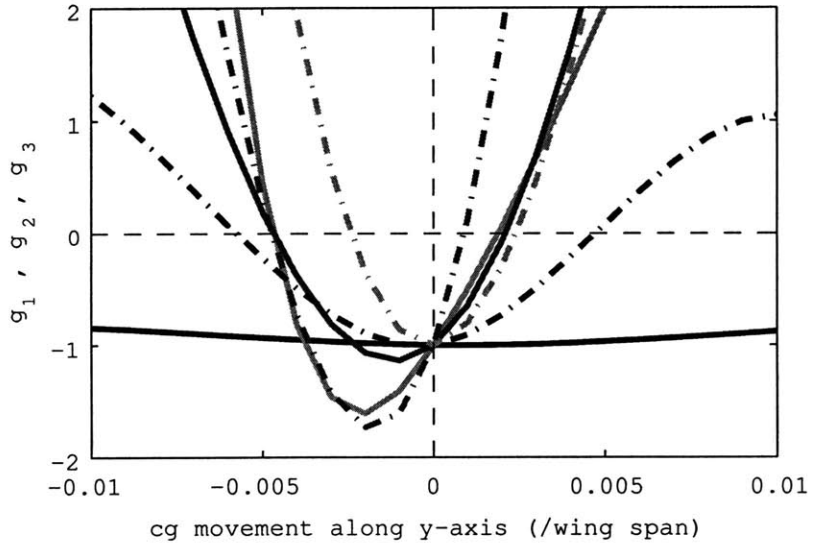

Figure 5-3: Case C: $g(\Delta_y/b_{ref})$ for the lateral FC.

As before, the adaptive controller has better robustness characteristics.

Unlike Case C, Case F considers an asymmetric aileron failure where λ_{a_1} is uncertain and $\lambda_{a_2} = 1$. Figure 5-6 illustrates the dependency of g on λ_{a_1} for both controllers. While the PSM for the baseline is 14%, the PSM for the adaptive is 20%. Consistently, the tracking performance requirement remains being critical. We note however that the PSM corresponding to the stability requirement for the adaptive controller becomes smaller.

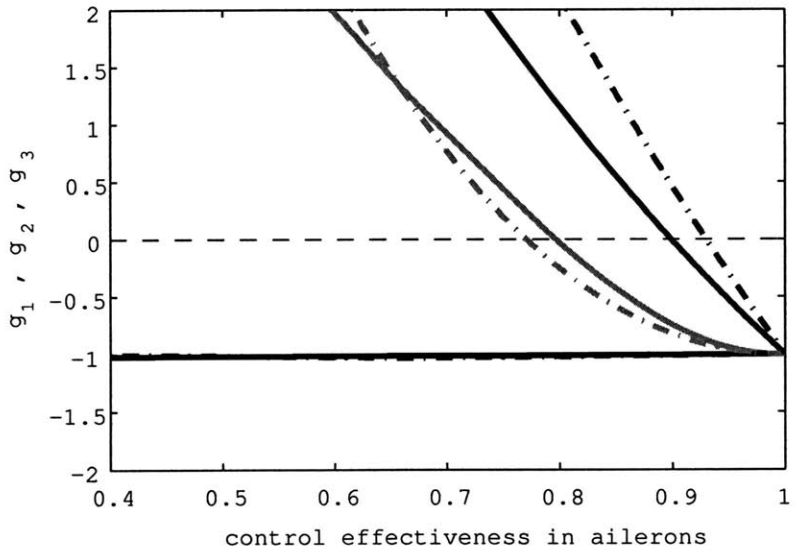

Figure 5-4: Case D: $g(\Lambda_{ail})$ for the lateral FC.

In Case G we consider a failure in the left outboard engine λ_{t1} for the longitudinal flight condition. Figure 5-7 illustrates the dependency of g on λ_{t1} for both controllers. While the PSM for the baseline is 1.7%, the PSM for the adaptive is 2.9%. As before, the tracking performance is the critical requirement. We note that the margins obtained in this case are considerably smaller than those found in the other cases. The non-failure domains are small since the throttle inputs are not controlled and remain fixed at their trim values. Results similar to those in Figure 5-7 were observed when the lateral flight condition was used.

A lock-in-place failure in the left elevator is considered in Case H. This is simulated by keeping this control input at a constant value for a period of t_l seconds. The larger

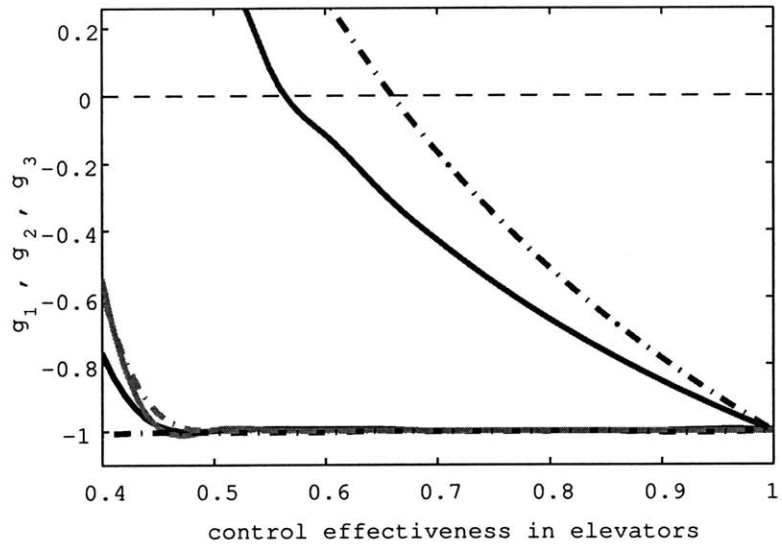

Figure 5-5: Case E: $g(\Lambda_{ele})$ for the longitudinal FC.

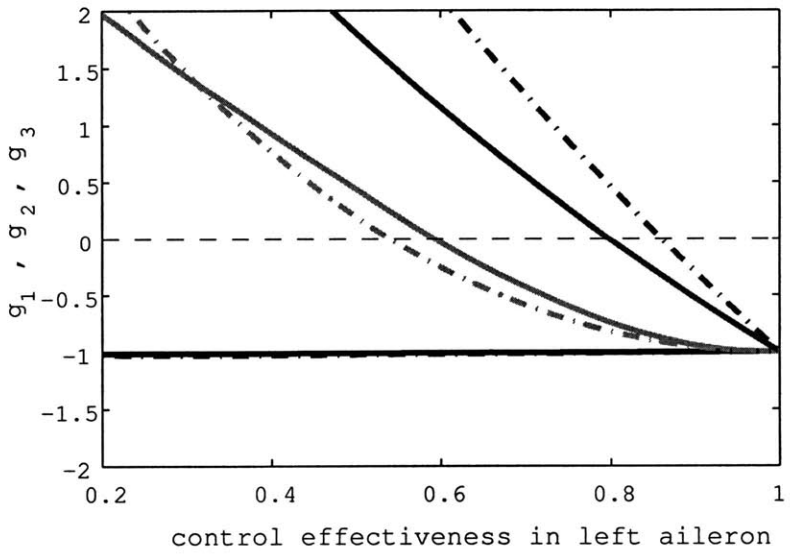

Figure 5-6: Case F: $g(\lambda_{a_1})$ for the lateral FC.

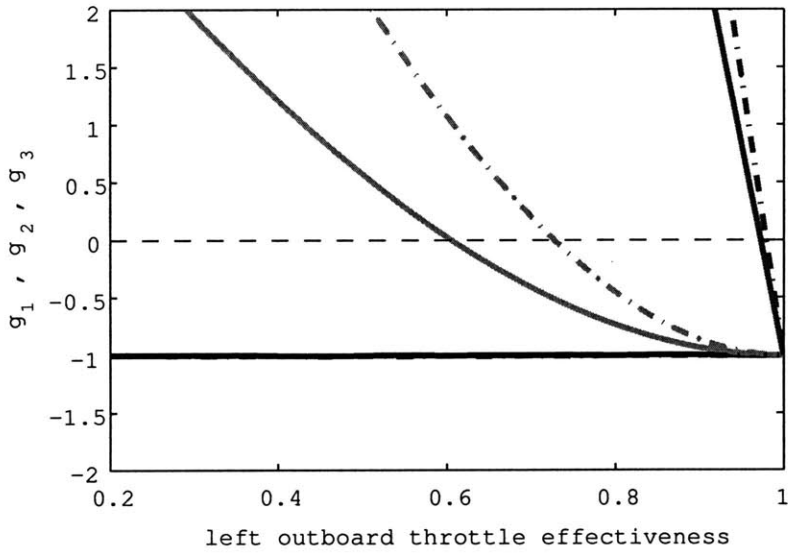

Figure 5-7: Case G: $g(\lambda_{t1})$ for the longitudinal FC.

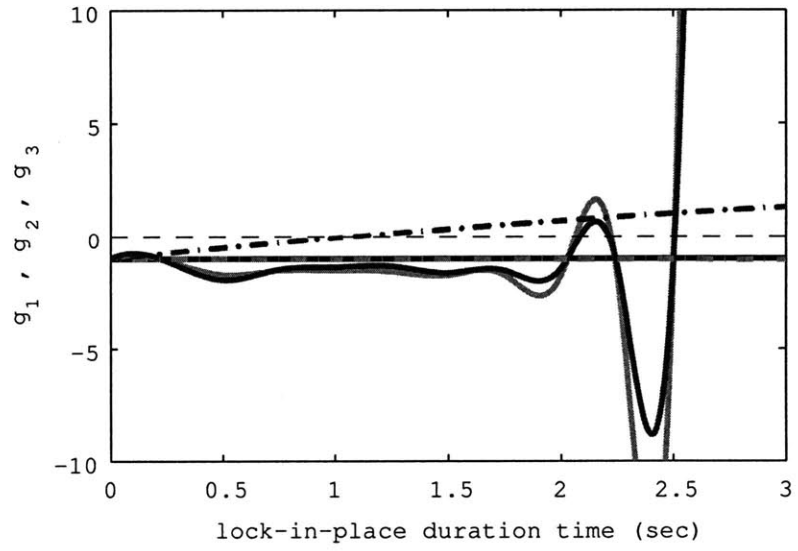

Figure 5-8: Case H: $g(t_l)$ for the longitudinal FC.

the t_l the more severe the failure. Figure 5-8 illustrates the dependency of g on the lock-in time. Substantial differences in the functional dependencies are apparent. It can be seen that the PSM for the baseline is 1.1 while the PSM for the adaptive is 2.1. We also note that while the tracking performance is critical for the baseline controller, the stability requirement is critical for the adaptive one.

Case I considers the case when there is a time delay τ in all three control inputs. Figure 5-9 illustrates the dependency of g on this uncertain parameter for the longitudinal flight condition. In contrast to all other cases, the non-failure domain of the adaptive controller is smaller than that of the baseline. Hence, the nominal controller is more robust to uncertainty in the time delay than the adaptive one. One may infer that this is the price of attaining improved system performance through aggressive actuation. We however note that this observation may not hold when multiple uncertainties occur simultaneously. Figure 5-10 shows time responses for both controllers when $\tau = 0.74$s. This point belongs to the non-failure domain of the baseline controller and to the failure domain of the adaptive one.

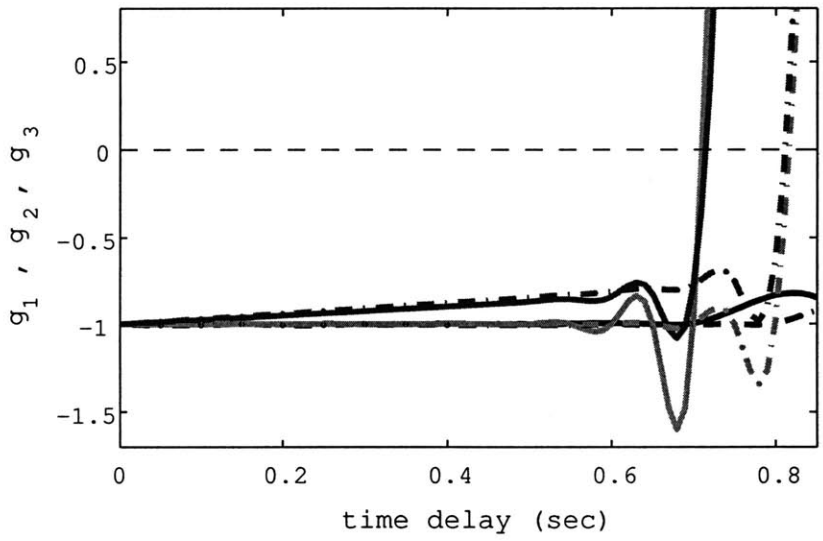

Figure 5-9: Case I: $g(\tau)$ for the longitudinal FC.

Table 5.3 summarizes the results above by presenting the relative change in PSM

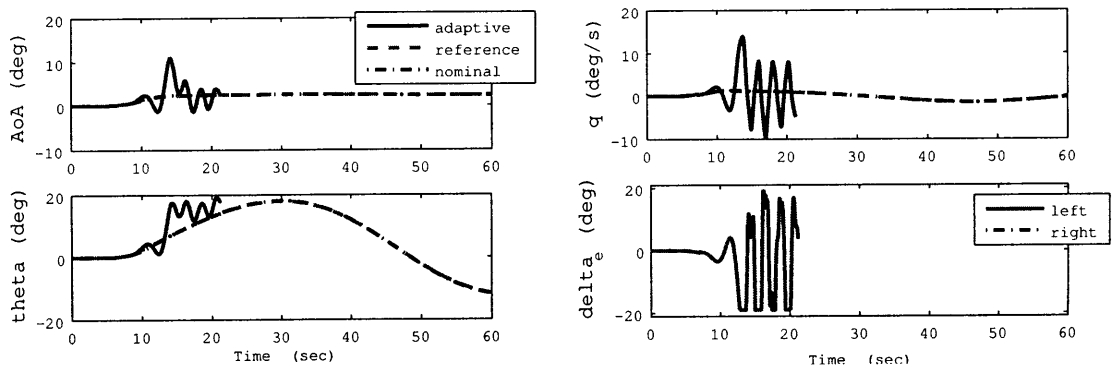

Figure 5-10: Time simulation for $\tau = 0.74$s.

Table 5.3: Summary for the results of all cases

Case	$\left(\frac{\rho_{adap}}{\rho_{base}} - 1\right) \times 100\%$	Critical Requirement
A	+4.01 %	g_1, g_3
B	+11.4 %	g_2, g_3
C	+133 %	g_2, g_3
D	+63.6 %	g_3
E	+27.3%	g_3
F	+46.7 %	g_3
G	+70.6 %	g_3
H	+88.9 %	g_2, g_3
I	-13.9 %	g_2, g_3

attained by the adaptive controller and the critical requirement. In all but one of the cases considered, the adaptive controller attains better robustness by a sizable margin.

5.2 Multi-dimensional Case

In all the cases above only a single uncertain parameter has been considered. In this setting, the effect of the dependencies among parameters can not be captured. The same analysis can be conducted for a multi-dimensional vector p. In such a case, multiple failures and uncertainties occur simultaneously and the correlation among them may play a significant role. Studies of this type will be presented elsewhere. However, Figure 5-11 presents a time simulation of the controlled response for a multi-

dimensional parameter realization when 2 pitch doublets are commanded. Therein, we assume losses in control effectiveness of 30% for the elevators, 10% for the ailerons, and 10% for the rudders. Besides, the CG has been moved to the left by $0.004/c_{ref}$, and a flight upset in the angle of attack of 0.2 degrees is assumed. It is apparent that the adaptive controller achieves good tracking performance while the nominal controller can not recover and makes the system unstable.

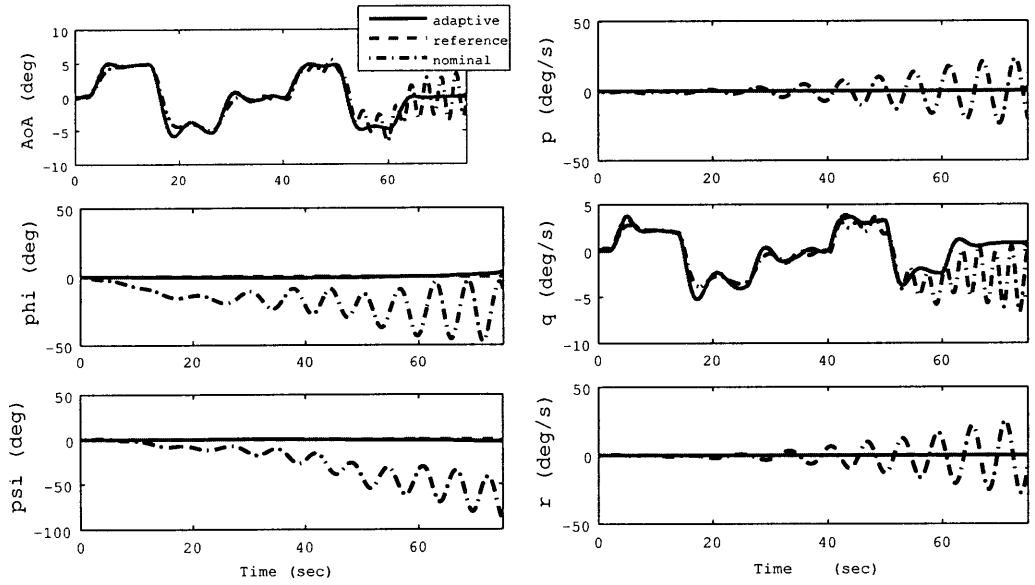

Figure 5-11: Time simulation for multiple uncertainties.

Chapter 6

Adaptive Control Design for the Generic Transport Model

In this chapter we focus on the development, implementation of adaptive control technology for the Generic Transport Model (GTM). In particular, we design a controller for the GTM and study improvements resulting from adaptation when various uncertainties and failures occur. The GTM is a dynamically scaled model of a transport aircraft for which NASA Langley has developed a high-fidelity simulink model. This simulation uses non-linear aerodynamic models extracted from wind tunnel data, and considers avionics, sensor dynamics, engine dynamics, atmospheric models, sensor noise and bias, telemetry effects, etc. This aircraft has ten controllable inputs and overall the open-loop plant has 278 states.

The adaptive control architecture consists of three major components, (i) a baseline controller that provides satisfactory performance under nominal flying conditions, (ii) an adaptive controller that accommodates for anomalies resulting from uncertainty and failure, and (iii) a partially nonlinear reference model designed according to the GTM dynamics. While the baseline controller is based on a control allocation scheme that correlates inputs, the adaptive controller accommodates for control saturation and integration wind-up without enforcing any allocation, which enables inputs to be independent. A significant improvement in flight safety introduced by the suggested control design is studied with several failure and damage cases.

6.1 Control Design

Again we start with the overall system dynamics which can be represented as

$$\dot{X} = F(X, \Lambda U) \tag{6.1}$$

where X is the state, U is the input, and Λ is the control effectiveness matrix. For control design purposes, this nonlinear plant is linearized about a trim point (X_0, U_0) satisfying $F(X_0, U_0) = 0$. Deviations from the trim values X_0 and U_0 will be written as lowercase letters in the developments that follow, e.g., $X = X_0 + x_p$ and $U = U_0 + u$. Linearization about the trim point leads to the LTI system

$$\dot{x_p} = A_p x_p + B_p \Lambda u + h(x_p, u) \tag{6.2}$$

where

$$A_p = \left.\frac{\partial F(X, \Lambda U)}{\partial X}\right|_{X_0,\, U_0}, \quad B_p = \left.\frac{\partial F(X, \Lambda U)}{\partial U}\right|_{X_0,\, U_0}, \tag{6.3}$$

and $h(x_p, u)$ contains higher order terms. After ignoring high order terms, this model can be written as

$$\dot{x}_p = A_p(\hat{p}) x_p + B_1 \Lambda(\hat{p})(R_s(u) + d) + B_2 \hat{r} \tag{6.4}$$

where A_p and Λ are unknown matrices, d is an exogenous disturbance, $\bar{r}$ is the reference input, and $R_s(u)$ is a saturation function. The state x is

$$x = [\alpha \ \beta \ V \ p \ q \ r \ x \ y \ z \ \phi \ \theta \ \psi]^T \tag{6.5}$$

which are angle of attack, sideslip angle, true aerodynamic speed, roll rate, pitch rate, yaw rate, longitude, latitude, altitude, and the three Euler angles [20]. The input u is

$$u = [\delta_{e_{LO}} \ \delta_{e_{LI}} \ \delta_{e_{RO}} \ \delta_{e_{RI}} \ \delta_{a_L} \ \delta_{a_R} \ \delta_{r_U} \ \delta_{r_L} \ \delta_{th_L} \ \delta_{th_R}]^T \tag{6.6}$$

which are the outer-left elevator, the inner-left elevator, the outer-right elevator, the inner-right elevator, the left aileron, the right aileron, the upper rudder, the lower rudder, the left engine throttle and the right engine throttle, respectively. The reference command r is

$$r = [\alpha_{\text{cmd}} \ \beta_{\text{cmd}} \ p_{\text{cmd}} \ V_{\text{cmd}}]^T \tag{6.7}$$

which are angle of attack-, sideslip-, roll rate- and true aerodynamic speed-commands. These four commands are used by the pilot to attain the desired flight maneuvers.

The sources of unknown time-delay in the control input τ are both known (e.g., telemetry, signal processing) and unknown (e.g., sensor failure, asynchronous communication).

The overall control architecture includes a baseline controller that is augmented by an adaptive component. While the baseline controller provides satisfactory performance in the absence of adverse conditions and uncertainties, the adaptive controller accommodates for them. Both controllers are based on a single trim point design. The point attains horizontal flight for a true aerodynamic speed of 80 knots, an altitude of 625.48ft, and a zero path angle.

6.1.1 Baseline Controller

The nominal controller consist of three controllers for the longitudinal dynamics, the lateral/directional dynamics, and the auto-throttle, depending on fast and slow states in the vehicle dynamics. LQR-PI architectures with integral actions corresponding to each of the reference command r are used. Anti-windup schemes for each error integral state are included to prevent undesired responses due to actuator saturation. A control allocation that correlates inputs to the same devices actually makes only four are independent out of the ten plant inputs. (i.e., elevator input δ_e, aileron input δ_a, rudder input δ_r, and throttle input δ_{th}).

Longitudinal Controller

The plant in the longitudinal axis of the aircraft is described as

$$\dot{x}_{\text{lon}} = A_{\text{lon}} x_{\text{lon}} + B_{\text{lon}} \delta_e \tag{6.8}$$

where $A_{\text{lon}} \in \mathbb{R}^{2\times 2}$ is the system matrix, $B_{\text{lon}} \in \mathbb{R}^{2\times 1}$ is the input matrix, and $x_{\text{lon}} = [\alpha \; q]^\top$ is the state. In order to follow a command in angle of attack, the integral error state is added.

$$e_\alpha = \int (\alpha - \alpha_{\text{cmd}}) dt \tag{6.9}$$

This leads to the augmented plant

$$\begin{bmatrix} \dot{x}_{\text{lon}} \\ \dot{e}_\alpha \end{bmatrix} = \begin{bmatrix} A_{\text{lon}} & 0 \\ H_1 & 0 \end{bmatrix} \begin{bmatrix} x_{\text{lon}} \\ e_\alpha \end{bmatrix} + \begin{bmatrix} B_{\text{lon}} \\ 0 \end{bmatrix} \delta_e + \begin{bmatrix} 0 \\ -1 \end{bmatrix} \alpha_{\text{cmd}} \tag{6.10}$$

Since the states in Equation (6.10) are accessible, an LQR controller that minimizes

$$J = \int (x^T Q x + u^T R u) dt, \tag{6.11}$$

where $Q = Q^\top \geq 0$, $R = R^\top > 0$ are weighting matrices, is designed. This leads to

$$\delta_e = \begin{bmatrix} K_{\text{lon}}^\top & k_{\delta_{e_\alpha}} \end{bmatrix} \begin{bmatrix} x_{\text{lon}} \\ e_\alpha \end{bmatrix} \tag{6.12}$$

This controller is designed so that it attains enough stability margins with which the inclusion of the low-pass and anti-aliasing filters in the sensors and the 40ms input delay caused by telemetry do not compromise closed-loop stability and performance.

The actual input to the plant is given by the saturation function

$$R_s(u) = \begin{cases} u & \text{if } u_{min} < u < u_{max}, \\ u_{max} & \text{if } u \geq u_{max}, \\ u_{min} & \text{otherwise} \end{cases} \tag{6.13}$$

In particular, $u = \delta_e$, $u_{max} = \delta_{e,max}$ and $u_{min} = \delta_{e,min}$ for the longitudinal controller. The control deficiency is given by

$$u_\Delta = R_s(u) - u. \tag{6.14}$$

The controller proposed uses an anti-windup technique. The aim of anti-windup compensation is to modify the dynamics of a control loop during control saturation so that an improved transient behavior is attained after the system leaves saturation. It was observed that the anti-windup technique chosen tends to prevent the growth of u by imposing virtual saturation limits on the error integral state used for feedback. This time-varying saturation function is described as

$$R_e(e_\alpha, \delta_e) = \begin{cases} e_\alpha & \text{if } R_2 \leq e_\alpha \leq R_1, \\ R_1 & \text{if } R_1 \leq e_\alpha, \\ R_2 & \text{if } e_\alpha \leq R_2. \end{cases} \tag{6.15}$$

where the limits R_1, R_2 are given by

$$\begin{aligned} R_1 &= \max\left[0, \frac{R_s(\delta_e) - (\Delta_e + K_{\text{lon}}^\top x_{\text{lon}})}{k_{\delta_{e_\alpha}}}, \frac{-R_s(\delta_e) - (\Delta_e + K_{\text{lon}}^\top x_{\text{lon}})}{k_{\delta_{e_\alpha}}}\right] \\ R_2 &= \min\left[0, \frac{R_s(\delta_e) - (\Delta_e + K_{\text{lon}}^\top x_{\text{lon}})}{k_{\delta_{e_\alpha}}}, \frac{-R_s(\delta_e) - (\Delta_e + K_{\text{lon}}^\top x_{\text{lon}})}{k_{\delta_{e_\alpha}}}\right] \end{aligned} \tag{6.16}$$

where Δ_e is elevator deflection at trim. Figure 6-1 illustrates the logic behind this technique. When the input saturates at $t = t_1$, the feedback term depending on the integral error state is $k_{\delta_{e_\alpha}} R_1$. At $t = t_2$, $\dot{e}_\alpha$ is equal to zero and the value of e_α is reset

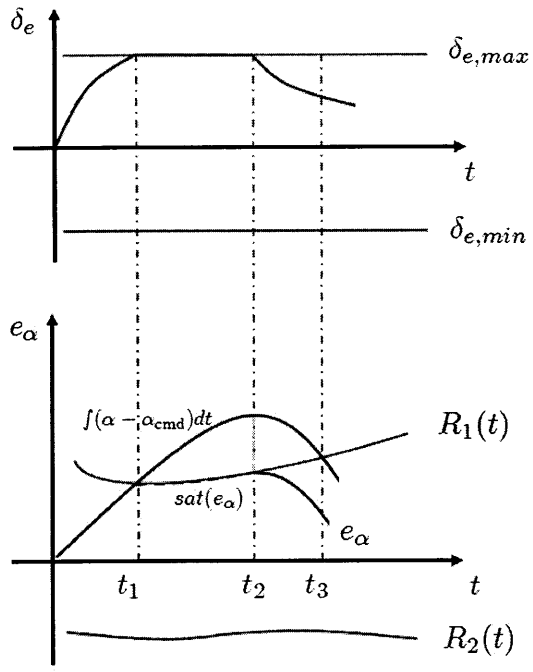

Figure 6-1: Anti-wind up technique for e_α and δ_e.

to the active virtual limit. A resetting action taken at time t_{ri} is defined as

$$e_\alpha(t_{ri}^+) = R_i \tag{6.17}$$

where t_{ri} is the time instant at which

$$\begin{aligned} &(a) \quad \|\delta_e(t_{ri})\| \leq \delta_{e,min} \text{ or } \delta_{e,max} \leq \|\delta_e(t_{ri})\| \text{ and} \\ &(b) \quad \dot{e_\alpha}(t_{ri}) = 0 \end{aligned} \tag{6.18}$$

and R_i is the virtual limit which is active at $t = t_{ri}$. Then the output of the controller is

$$\delta_e = \begin{bmatrix} K_{\text{lon}}^\top & k_{\delta_{e_\alpha}} \end{bmatrix} \begin{bmatrix} x_{\text{lon}} \\ R(e_\alpha, \delta_e) \end{bmatrix} \tag{6.19}$$

This technique usually leads to shorter input saturation periods, and smaller input

rates after the system leaves saturation. The error deficiency is

$$e_{\alpha,\Delta} = R_e(e_\alpha, \delta_e) - e_\alpha. \tag{6.20}$$

The resulting linear time varying (LTV) system which describes the closed-loop longitudinal dynamics is given by

$$\begin{bmatrix} \dot{x}_{\text{lon}} \\ \dot{e}_\alpha \end{bmatrix} = \begin{bmatrix} A_{\text{lon}} + B_{\text{lon}} K_{\text{lon}}^\top & B_{\text{lon}} k_{\delta_{e_\alpha}} \\ H_1 & 0 \end{bmatrix} \begin{bmatrix} x_{\text{lon}} \\ e_\alpha \end{bmatrix} + \begin{bmatrix} B_{\text{lon}} \\ 0 \end{bmatrix} (u_\Delta + k_{\delta_{e_\alpha}} e_{\alpha,\Delta}) + \begin{bmatrix} 0 \\ -1 \end{bmatrix} \alpha_{\text{cmd}} \tag{6.21}$$

with (6.17). The boundedness of the system can be established for all initial conditions inside a bounded set. This bounded set extends to the entire state-space when the open-loop plant is stable and there is no unmodeled dynamics [24].

Lateral/Directional Controller

The LTI model of the plant is

$$\dot{x}_{\text{lat}} = A_{\text{lat}} x_{\text{lat}} + B_{\text{lat}} u_{\text{lat}} \tag{6.22}$$

where $A_{\text{lat}} \in \mathbb{R}^{3\times 3}$ is the system matrix, $B_{\text{lat}} \in \mathbb{R}^{3\times 2}$ is the input matrix, $x_{\text{lat}} = [\beta\ p\ r]^\top$ is the state, and $u_{\text{lat}} = [\delta_a\ \delta_r]^\top$ is the input. To achieve the command following, error integral states for sideslip and roll rate which are given by

$$e_\beta = \int (\beta - \beta_{\text{cmd}}) dt \tag{6.23}$$

$$e_p = \int (p - p_{\text{cmd}}) dt \tag{6.24}$$

are added. The integral error in sideslip was chosen over that of the yaw rate to facilitate the generation of commands for coordinated turns with non-zero bank angles

and for cross-wind landing. The augmented plant is given by

$$\begin{bmatrix} \dot{x}_{\text{lat}} \\ \dot{e}_\beta \\ \dot{e}_p \end{bmatrix} = \begin{bmatrix} A_{\text{lat}} & 0 \\ H_2 & 0 \end{bmatrix} \begin{bmatrix} x_{\text{lat}} \\ e_\beta \\ e_p \end{bmatrix} + \begin{bmatrix} B_{\text{lat}} \\ 0 \end{bmatrix} u_{\text{lat}} + \begin{bmatrix} 0 \\ -I \end{bmatrix} \begin{bmatrix} \beta_{\text{cmd}} \\ p_{\text{cmd}} \end{bmatrix} \tag{6.25}$$

A LQR-PI control structure is adopted, which leads to

$$\begin{bmatrix} \delta_a \\ \delta_r \end{bmatrix} = \begin{bmatrix} K_{\text{lat}}^\top & K_{e_\beta}^\top & K_{e_p}^\top \end{bmatrix} \begin{bmatrix} x_{\text{lat}} \\ e_\beta \\ e_p \end{bmatrix} \tag{6.26}$$

As before, the controller is design so that its stability margins can accommodate for the filters in the sensors and the time delay. The anti-windup technique presented in Section 6.1.1 which are exemplified with the pair of $\langle e_\alpha, \delta_e \rangle$ is also applied to $\langle e_\beta, \delta_r \rangle$ and $\langle e_p, \delta_a \rangle$.

Auto-throttle

The auto-throttle helps the pilot to attain a desired airspeed by controlling the total thrust. A PID structure having the integral error

$$e_V = \int (V - V_{\text{cmd}}) dt \tag{6.27}$$

as input is used. This leads to

$$\delta_{th} = \begin{bmatrix} k_P & k_I & k_D \end{bmatrix} \begin{bmatrix} \dot{e_V} \\ e_V \\ \ddot{e_V} \end{bmatrix}, \tag{6.28}$$

where the gains are determined by the Ziegler-Nichols tuning rule. To reduce the sensitivity to noise in the airspeed, a first-order lag is added to the controller and $\ddot{e_V}$ is calculated using an approximate differentiator. The anti-windup technique

is applied herein to the pair of $\langle e_V, \delta_{th} \rangle$. We note that the slow engine dynamics, which contains a low-pass filter scheduled with the RPM of the turbine, makes the V response much slower than that of α, β, p, q, and r.

Control Allocation

Equations (6.12), (6.26), and (6.28), along with the four realizations of the anti-windup technique, prescribe the input $u_n = [\delta_e \ \delta_a \ \delta_r \ \delta_{th}]^\top$. This input along with a control allocation scheme fully determines the ten control inputs to the aircraft.

$$u_{\text{nom}} = G u_n = G K_n^\top x, \tag{6.29}$$

where G is the control allocation matrix, and K_n is the feedback gain designed. The allocation of u_n enforced by G is as follows. $\delta_{e_{LO}} = \delta_{e_{LI}} = \delta_{e_{RO}} = \delta_{e_{RI}} = \delta_e$, $-\delta_{a_L} = \delta_{a_R} = \delta_a$, $\delta_{r_U} = \delta_{r_L} = \delta_r$, and $\delta_{th_L} = \delta_{th_R} = \delta_{th}$.

6.1.2 Adaptive Controller

The adaptive controller is augmented to the baseline controller to accommodate for adverse conditions and uncertainties. The whole control signal is

$$u = u_{\text{nom}} + u_{\text{ada}} \tag{6.30}$$

where u_{nom} and u_{ada} are the inputs corresponding to the baseline and adaptive controllers. In contrast to the baseline controller, the adaptive controller generates independent signals for each of the ten inputs. This enables the system to use the engines for attitude control when control surfaces fail. An immediate consequence of integrating the engines to the flight control system is the enlargement of the failure set where the vehicle remains controllable. We note that the LTI systems used to design the longitudinal and lateral/directional controllers are accurate approximations as long as coupling between the corresponding dynamics is weak. However, there might be present strong coupling due to the failures and uncertainties, e.g., both left elevators

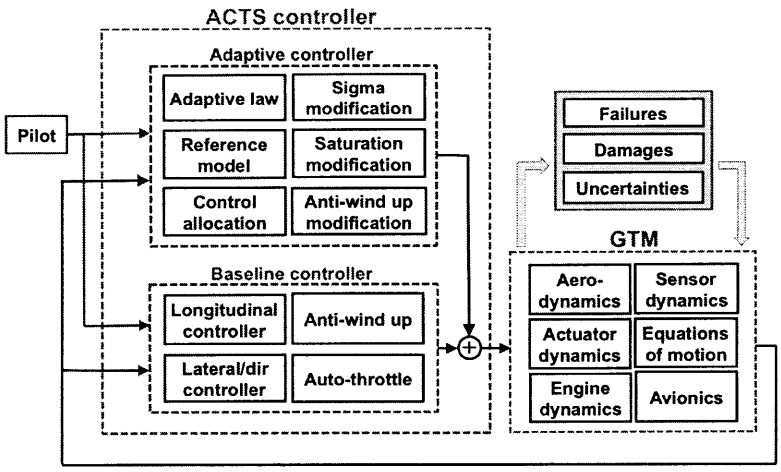

Figure 6-2: Control Architecture.

are locked-in-place with a non-zero deflection. In such a case, the adaptive component of the controller, whose underlying dynamic model is coupled, will be active. The adaptive controller designed is summarized in Fig, 6-2.

Reference Model

An LTI representation of the closed-loop system corresponding to the baseline controller under nominal flying conditions can be used as the reference model.

$$\dot{x}_m = \underbrace{\left[A_p + B_1 G K_n^\top\right]}_{A_m} x_m + B_m \hat{r} \tag{6.31}$$

where $A_m \in \mathbb{R}^{8\times 8}$, $B_m \in \mathbb{R}^{8\times 3}$, $x_m = [\alpha\ \beta\ p\ q\ r\ e_\alpha\ e_\beta\ e_p]^\top$, and $\hat{r} = [\alpha_{\text{cmd}}\ \beta_{\text{cmd}}\ p_{\text{cmd}}]^\top$. This model captures the coupling between the longitudinal and lateral/directional dynamics. We note that a modified model which is not exactly the same as (6.31) is used when implementing, in order to accommodate for the negligible effect of nonlinearities. Details of the model which is actually implemented are discussed in Section 6.2.1.

Adaptive Law

The plant to be controlled is assumed as

$$\dot{x}_p = A_p x_p + B_1 \Lambda \left(R_s(u) + d \right) + B_2 \hat{r} \tag{6.32}$$

where $A_p \in \mathbb{R}^{8\times 8}$, $B_1 \in \mathbb{R}^{8\times 10}$, $\Lambda = \text{diag}(\lambda) \in \mathbb{R}^{10\times 10}$, and $B_2 \in \mathbb{R}^{8\times 3}$. The states, inputs, and commands in (6.32) are

$$\begin{aligned} x_p &= [x_{\text{lon}}^\top \; x_{\text{lat}}^\top \; e_\alpha \; e_\beta \; e_p]^\top \\ u &= [\delta_{e_{LO}} \; \delta_{e_{LI}} \; \delta_{e_{RO}} \; \delta_{e_{RI}} \; \delta_{a_L} \; \delta_{a_R} \; \delta_{r_U} \; \delta_{r_L} \; \delta_{th_L} \; \delta_{th_R}]^\top \\ r &= [\alpha_{\text{cmd}} \; \beta_{\text{cmd}} \; p_{\text{cmd}}]^\top \end{aligned} \tag{6.33}$$

while $d \in \mathbb{R}^{10\times 1}$ is a input disturbance.

The adaptive input with an anti-windup modification is given by

$$u_{\text{ada}} = \theta^\top \omega = \begin{bmatrix} \theta_x^\top & \theta_d \end{bmatrix} \begin{bmatrix} x_p \\ 1 \end{bmatrix} \tag{6.34}$$

where $\theta_x \in \mathbb{R}^{8\times 10}$, and $\theta_d \in \mathbb{R}^{1\times 10}$ are adaptive parameters. Defining the state error e as

$$e = x_p - x_m, \tag{6.35}$$

we choose the adaptive laws for adjusting the adaptive parameters in (6.34) as

$$\dot{\theta} = -\Gamma \omega e_u^\top P B_1 \text{sign}(\Lambda) - \sigma \theta \tag{6.36}$$

$$\dot{\hat{\lambda}} = -\Gamma_\lambda \text{diag}(\kappa) B_1^T P e_u \tag{6.37}$$

where $P = P^\top > 0$ with $A_m^\top P + P A_m = -Q, Q = Q^\top > 0$ and $e_u = e - e_\Delta$. To

accommodate for the control deficiencies (6.14), the auxiliary error e_Δ is defined as

$$\dot{e}_\Delta = A_m e_\Delta - B_1 \text{diag}\left(\hat{\lambda}\right) \kappa \tag{6.38}$$

$$\kappa = u_\Delta + (K_{e_\alpha}^T + \theta_{e_\alpha}^T) e_{\alpha,\Delta} \tag{6.39}$$

While e_Δ is the error caused by the saturations in the actuators and in e_α, e_u is the error due to uncertainties. The variables $\Gamma > 0$, $\Gamma_\lambda > 0$, and σ are design parameters that determine the speed of adaption.

It should be noted that the stability and boundedness of the closed-loop augmented system has been proved in [7, 11, 23] when physical saturation constraints are present. The stability analysis for the resetting-based anti-windup logic was also established and to be appeared in [meg10ACC].

6.2 Control Implementation

This section describes aspects of the implementation of the controller that depart from the LTI framework used for control design.

6.2.1 Reference Model

In contrast to developments made with LTI plants and reference models, which support most of the theoretical foundations of adaptive control, the GTM is a nonlinear model whose flight envelope extends beyond the region in the state space where a single LTI system is sufficiently accurate. As a consequence, even without any failure or uncertainties, the adaptive system with the linear reference model in Equation (6.31) attempts to minimize the tracking error by adjusting its gains. That is, due to the nonlinearities, the adaptive controller is activated even without any failure in the system. Therefore what is necessary are alternatives to the linear reference model in (6.31), in order to expand the range of accuracy of the reference model which leads to a desirable adaptation.

One choice is to combine the full non-linear model of the aircraft under nominal

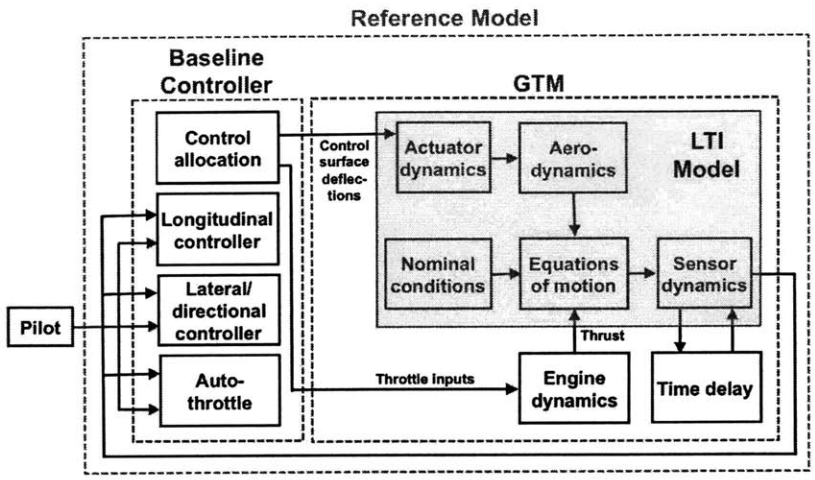

Figure 6-3: Reference model.

flying conditions with the baseline controller. Even though this is a very accurate model, its computational requirements are exceedingly high.

The search for a simple yet accurate reference model lead us to develop a LTI model with a nonlinear engine model where the states and inputs are $x = [\alpha\ \beta\ V\ p\ q\ r\ x\ y\ z\ \psi\ \theta\ \phi]^\top$ and $u = [\delta_e\ \delta_a\ \delta_r\ \delta_{th}]^\top$. Furthermore we include a 20ms input delay to all states due to the up-link and down-link, an additional 40ms to the Euler angles due to the MIDG sensor dynamics, anti-aliasing filters and command rate limiters.

It was observed in the simulation studies that this model is sufficiently accurate to describe the actual vehicle dynamics, in which the engine has a first-order lag whose time-constant is a nonlinear function of the engine RPMs and of the fuel dynamics. A sketch of the adopted reference model is shown in Figure 6-3. We note that only a subset of the states in this reference model is used as x_m in Equation (6.31). We also note that even though V is accurately represented by the reference model, it is not a state used in adaptation. This state is neglected because of its comparatively slow dynamics.

6.2.2 Adaptive Rate

In real systems there present nonlinearites and time delays. Therefore the robustness of the adaptive system to unmodelled dynamics has to be guaranteed. While small

adaptive gains diminish the performance, large adaptive gains reduce the robustness. The adaptive rate we choose for the suggested controller is based on the heuristic rule proposed in [13], and tuned further according to the closed-loop performance observed in simulation.

6.3 Case Studies

In this section we compare the performance of the baseline and adaptive controllers for a set of damages in the structure of the aircraft. The models of the first six cases are included in the GTM simulation code. In all cases, the aircraft is initially trimmed for a 45 deg bank angle turn with a flight path angle of 3 deg and an aerodynamic speed 95 knots. The damage occurs at $t = 5$. Throughout the simulation the commands keep the values they assumed at trim.

6.3.1 Rudders Off

This case is referred to as *Damaged Case* 1 in the GTM simulation code. This is a mild damage in which both rudders are off. As a result, the inertial properties of the vehicle (i.e., weight, CG location and inertia tensor) are altered, the aerodynamics of the airframe (e.g., $C_{N\beta}$, rolling moment, yawing moment and side force due yaw rate) change and the control effectiveness of both rudders becomes zero.

Figure 6-4 shows the time response of the states corresponding to (i) open-loop with no damage, (ii) open-loop with damage, (iii) closed-loop for the baseline controller with damage and (iv) closed-loop for the adaptive controller with damage. We note that the vehicle keeps climbing at the desired flight path angle when the controllers are on. We also note that even though the transient response of the baseline controller is slightly better than that of the adaptive controller, they converge to similar steady states. Throughout the simulation none of the control inputs saturate.

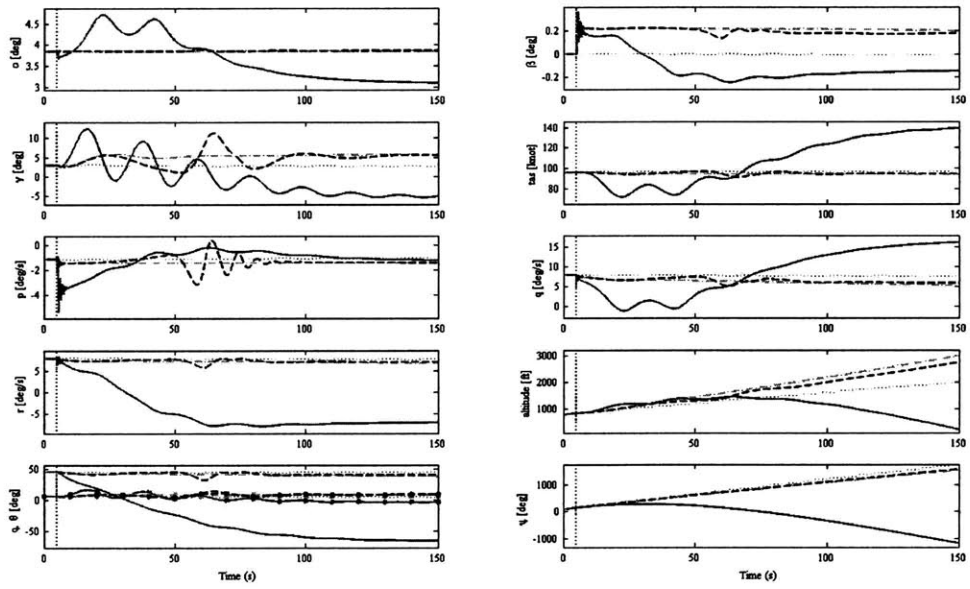

Figure 6-4: States: Time simulation for Rudders Off. Line conventions are as follows: open-loop response with no damage (green, short-dashed line), open-loop with damage (red, solid line), closed-loop for the baseline controller with damage (cyan, dot-dashed line), closed-loop for the adaptive controller with damage (blue long-dashed line).

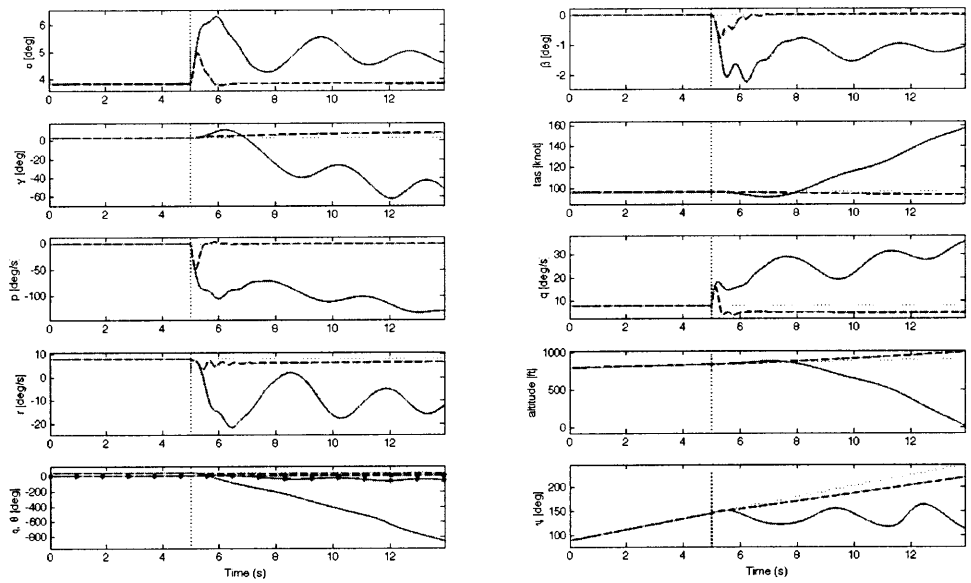

Figure 6-5: States: Time simulation for 25% Left Wingtip Off.

6.3.2 25% Left Wingtip Off

This case is referred to as *Damaged Case* 4. This is a mild damage in which 25% of the outboard left wing tip is lost. In this case the inertial properties of the vehicle are altered, the aerodynamics of the airframe (e.g., $C_{L\alpha}$, rolling moment from left wing) change and the effectiveness of the left aileron becomes zero. This damage generates residual roll moments that increase dynamic coupling. In Figure 6-5 we see that the effects of both controllers are practically indistinguishable and the vehicle is recovered without saturation. Figure 6-5 shows the time response of the states corresponding to the cases (i), (ii), (iii) and (iv).

6.3.3 Aft CG Shift

In this case the CG is moved aft 50% of the mean aerodynamic chord from its nominal location and the outer left elevator is locked-in-place at zero degree. While aft CG movements lower stability margins, the actuator failure couples the longitudinal and lateral/directional dynamics. In contrast to all previous damages, The improved

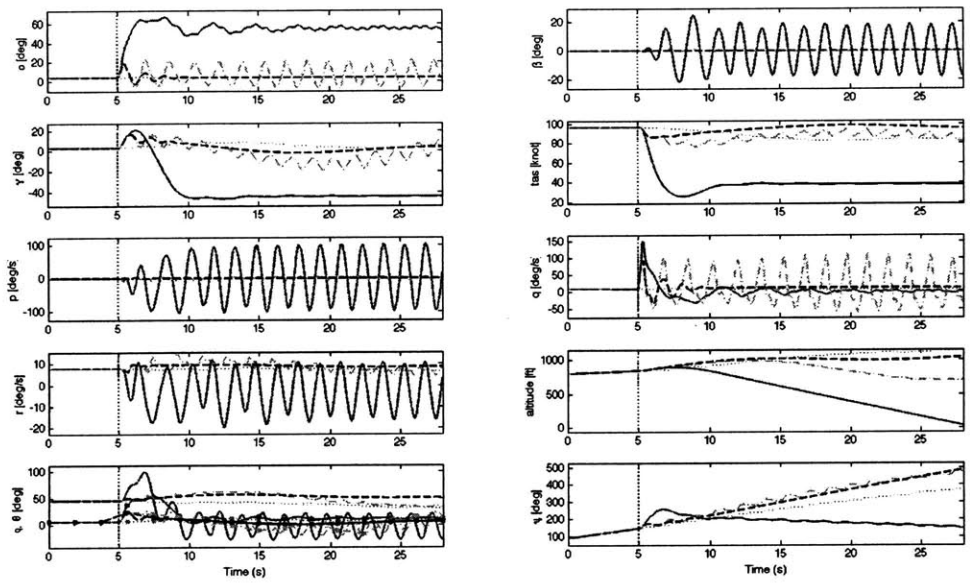

Figure 6-6: States: Time simulation for CG shift.

performance resulting from the adaptation is apparent. in this case. Figures 6-6, 6-7 and 6-8 show the closed-loop responses corresponding to the baseline and adaptive controllers. The adaptive controller suppresses the high frequency oscillations after a short transient. While the functioning elevators and throttle inputs corresponding to the baseline controller saturate repeatedly, those corresponding to the adaptive controller only do so during the transient. It is during this transient that most of the adaptation takes place. Figure 6-8 shows the left-right input differentials generated by the adaptive controller. Even though the magnitude of the differentials is small relative to the total control input deflection (with the exception of the ailerons for which the differential is about 50% of the deflection), they converge to non-zero values. This exemplifies a situation where the adaptive controller takes advantage of not allocating inputs.

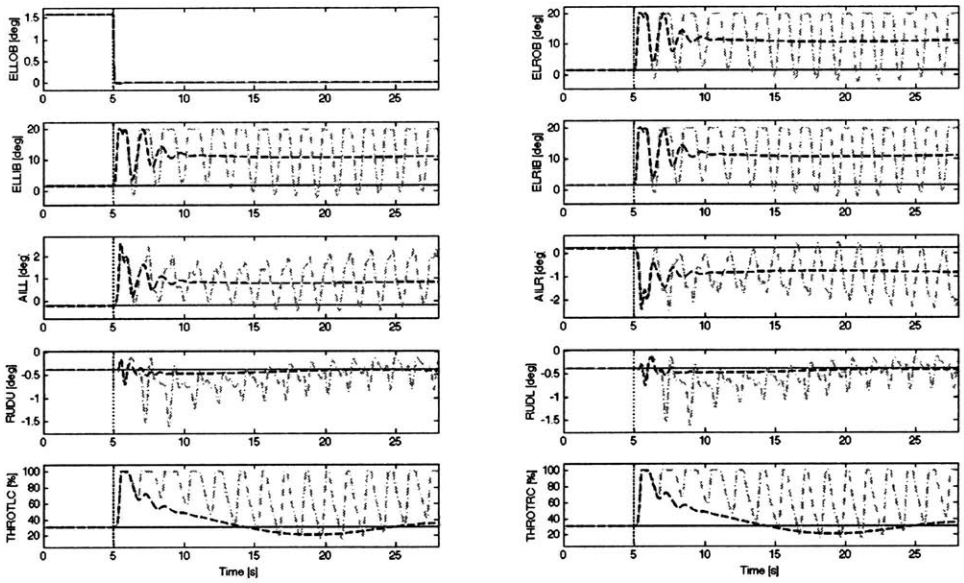

Figure 6-7: Inputs: Time simulation for CG shift.

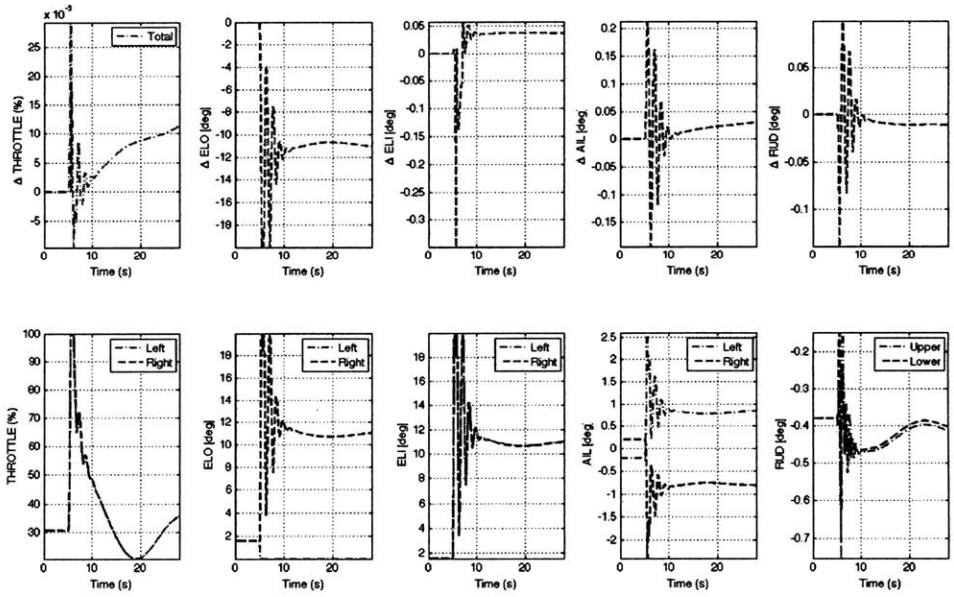

Figure 6-8: Input differentials: Time simulation for CG shift.

6.4 Conclusions and Remarks

This chapter proposes an adaptive control architecture for safe flight which is applied to the actual GTM. The most salient features of this controller are its ability to cope with control saturation and integration wind up. The case studies show that the proposed adaptive control architecture improves flight safety, which is almost a consistent result with the previous chapters. In particular, the robustness to CG shifts improves significantly. The robustness attained by the proposed controller is consistent with that of the controller designed to primarily accommodate for parametric uncertainty. It can be expected that other architectures targeting systems with large dynamic uncertainties, such as the time delay, may lead to further improvement in the performance in the presence of various uncertainties and damages.

A comparison between the controller designed and studied in the previous chapters and the one developed in this chapter is in order. The baseline controller designed for the GTM is further augmented with two more error integral states (e_β and e_p), which improve the performance in the lateral/directional axes. As a result, the performance of the adaptive controller gets indistinguishable from that of the baseline in the cases of Rudders Off and 25% Left Wingtip Off.

Chapter 7

Summary

The challenge of achieving safe flight comes into sharp focus in the face of adverse conditions caused by faults, damage, or upsets. A technology that has the potential for enabling a safe flight under these adverse conditions is adaptive control. One of the main features of an adaptive control architecture is its ability to react to changing characteristics of the underlying plant dynamics. Even its ability to deal with uncertainties which belong to certain families in the system are well known and proven both theoretically and analytically, it remains to be determined whether the adaptive control technology truly meaningful to be adopted in the aerospace applications to achieve the safety flight. This thesis addresses this question by performing a comparative analysis of the robustness of the best non-adaptive controller with its adaptive augmentation.

The adaptive control architecture is proposed by augmenting the baseline controller which consists of a longitudinal, and a lateral/directional controller with the adaptive components. While the baseline controller uses anti-wind up devices and a control allocation scheme that correlates inputs of the same class, the adaptive controller accommodates for control saturation and integration wind-up without enforcing any allocation. This leads to an architecture where each control input is actuated independently.

The stand-alone control verification framework is used, for evaluating the degradation in closed-loop performance caused by increasingly larger values of uncertainty

by attaining the set in the uncertain parameter space for which a set of closed-loop requirements are satisfied. This thesis studies several one-dimensional uncertainty analyzes for two flight maneuvers that focus on the longitudinal and lateral dynamics. As compared to the baseline controller, the adaptive controller enlarges the region of safe operation by a sizable margin in all but one of the cases considered. We therefore can conclude that the adaptive control technology realizes the system with the increased robustness to uncertainties. We note that this framework also enables us to assess and compare different advanced controller alternatives to achieve the safety flight, regardless of the methods, assumptions, and control structure used to derive them.

Finally, this thesis also proposes an actual adaptive control architecture for the GTM. Since this model, as the vehicle itself, departs considerably from the Linear Time Invariant (LTI) system usually assumed for control design, it remains to be determined if the improvements in stability, safety, and performance observed in such an assumption can be realized in practice. Several case studies show that the adaptive control enables the system to regain the nominal flight even with the severe failure such as CG movement, which is the consistent result with the proceeding studies based on C-5 aircraft model. Based on the suggested adaptive control design, conducting a flight test is also on our research road map. As well as the studies conducted in this thesis, this strongly connects this mature theoretical discipline of adaptive control to the actual world, and leads to realization of actual applications of adaptive control on aerospace applications to achieve a safety flight.

Bibliography

[1] K. J. Åström and B. Wittenmark. *Adaptive Control, 2nd ed.* Addison-Wesley, Reading, MA, 1995.

[2] P. A. Ioannou and J. Sun. *Robust Adaptive Control.* Prentice-Hall, Upper Saddle River, NJ, 1996.

[3] I. D. Landau. *Adaptive Control: The Model Reference Approach.* Marcel Dekker, New York, NY, 1979.

[4] K. S. Narendra and A. M. Annaswamy. *Stable Adaptive Systems.* Prentice-Hall, Englewood Cliffs, NJ, 1989.

[5] S. Sastry and M. Bodson. *Adaptive Control: Stability, Convergence, and Robustness.* Prentice-Hall, Englewood Cliffs, NJ, 1994.

[6] H. K. Khalil. *Nonlinear Systems.* Prentice-Hall, Upper Saddle River, NJ, 1996.

[7] S. P. Karason and A. M. Annaswamy. Adaptive control in the presence of input constraints. *IEEE Transaction on Automatic Control*, 46(11):2325–2330, November 1994.

[8] M. Schwager, H. Jain, A. M. Annaswamy, and E. Lavretsky. Towards verifiable adaptive flight control for safety critical applications. In *Proc. AIAA Guidance, Navigation, and Control Conference*, San Francisco, CA, Aug 2005.

[9] H. Jain, Z. T. Dydek, J. Jang, A. M. Annaswamy, and E. Lavretsky. Optimal selection of the free design parameters in an adaptive controller. In *Proc. AIAA Guidance, Navigation, and Control Conference*, Keystone, CO, Aug 2006.

[10] M. Schwager, A. M. Annaswamy, and E. Lavretsky. Adaptation-based reconfiguration in the presence of actuator failures and saturation. In *Proc. American Control Conference*, pages 2640–2645, Portland, Oregon, June 2005.

[11] M. Schwager and A. M. Annaswamy. Adaptive control of multi-input systems with magnitude saturation constraints. In *Proc. Conference on Decision and Control*, pages 783–788, Seville, Spain, December 2005.

[12] J. Jang, A. M. Annaswamy, and E. Lavretsky. Towards verifiable adaptive flight control in the presence of actuator anomalies. In *Proc. Conference on Decision and Control*, pages 3300–3305, San Diego, California, December 2006.

[13] Z. T. Dydek, H. Jain, J. Jang, A. M. Annaswamy, and E.Lavretsky. Theoretically verifiable stability margins for an adaptive controller. In *Proc. AIAA Conference on Guidance, Navigation, and Control*, Keystone, Colorado, August 2006. AIAA-2006-6416.

[14] R. M. Bailey, R. W. Hostetler, K. N. Barnes, and C. M. Belcastro. Experimental validation: Subscal aircraft ground facilities and integrated test capability. In *AIAA Guidance, Navigation, and Control Conference*, 2005. AIAA-2005-6433.

[15] B. J. Bacon and I. M. Gregory. General equations of motion for a damaged asymmetric aircraft. In *AIAA Atmospheric Flight Mechanics Conference and Exhibit*, Hilton Head, South Carolina, August 2007. AIAA-2007-6306.

[16] L. G. Crespo, D. P. Giesy, and S. P. Kenny. Figures of merit for control verification. In *AIAA-2008-6339*, August 2008.

[17] K. S. Tsakalis and P. A. Ioannou. *Linear Time-Varying Systems: Control and Adaptation.* Prentice Hall, Englewood Cliffs, NJ, 1992.

[18] L. G. Crespo, D. P. Giesy, and S. P. Kenny. Robust analysis and robust design of uncertain systems. *AIAA Journal*, 46(2), 2008.

[19] R. K. Heffley and W. F. Jewell. Aircraft handling qualities data. Contractor's Report CR-2144, NASA, Systems Technology, Inc. Hawthorne, CA 90250, December 1972. Available at ntrs.nasa.gov.

[20] B. Stevens and F. Lewis. *Aircraft Control and Simulation, 2nd Edition.* Wiley-Interscience, Reston, 2003.

[21] R. C. Nelson. *Flight Stability and Automatic Control.* McGraw-Hill, 1989.

[22] J. Jang, A. M. Annaswamy, and E. Lavretsky. Adaptive flight control in the presence of multiple actuator anomalies. In *American Control Conference*, pages 3300–3305, New York, NY, 2007.

[23] J. Jang, A. M. Annaswamy, and E. Lavretsky. Adaptive flight control in the presence of multi-input magnitude saturation. In *American Control Conference*, 2008.

[24] M. Matsutani, L. G. Crespo, and A. M. Annaswamy. An adaptive control technology for safety of a gtm-like aircraft. TC 000000, NASA, NASA Langley Research Center, Hampton, VA, 2009. In review.